



23 **ABSTRACT**

24 This paper presents a concept for parametric modelling of mechanized tunnelling within a state of  
25 the art design environment, as the basis for design assessments for different levels of details (LoDs).  
26 To this end, a parametric representation of each system component (soil with excavation, tunnel  
27 lining with grouting, Tunnel Boring Machine (TBM) and buildings) is developed in an information  
28 model for three LoDs (high, medium and low) and used for the automated generation of numerical  
29 models of the tunnel construction process and soil-structure interaction. The platform enables a  
30 flexible, user-friendly generation of the tunnel structure for arbitrary alignments based on  
31 predefined structural templates for each component, supporting the design process and at the same  
32 time providing an insight into the stability and safety of the design. This model, with selected  
33 optimal LoDs for each component, dependent on the objective of the analysis, is used for efficient  
34 design and process optimisation in mechanized tunnelling. Efficiency and accuracy are further  
35 demonstrated through an error-free exchange of information between Building Information  
36 Modelling (BIM) and the numerical simulation and with significantly reduced computational effort.  
37 The interoperability of the proposed multi-level framework is enabled through the use of an  
38 efficient multi-level representation context of the Industry Foundation Classes (IFC). The results  
39 reveal that this approach is a major step towards sensible modelling and numerical analysis of  
40 complex tunnelling project information at the early design stages.

41

42 **KEYWORDS**

43 Building Information Modelling; Industry Foundation Classes, mechanised tunnelling; multi-level  
44 modelling; numerical simulation; visualisation

45 **1. INTRODUCTION**

46 With increasing urbanisation and mobility, the need for underground tunnel facilities becomes  
47 evident. The efficient and safe design and construction of mechanised tunnels involves complex  
48 data management incorporating information not only about the tunnel structure, but also about the  
49 existing built infrastructure, the ground and the boring machine. In early design phases, crucial  
50 decisions have to be made, for example, on the alignment of the tunnel track in order to minimise  
51 the risks of settlement induced damage to existing buildings. This task can now be supported by  
52 sophisticated, process-oriented finite element (FE) analysis. However, the required FE models are  
53 characterised by a high degree of detail at high costs of preparation and computational effort  
54 preventing them from being readily applied during what-if scenario analyses at early design stages.  
55 The appraisal of different design alternatives is essential for ensuring optimal designs. Assessing  
56 the effects of various alternatives for tunnelling projects on the surrounding environment is a multi-  
57 disciplinary and complex problem. The current state of the art process is cumbersome and requires  
58 significant computing resources and time (sophisticated simulations including all details can take  
59 days or weeks to complete). This often leads to sub-optimal solutions which are not optimal in their  
60 effect on the existing infrastructure. However, at the conceptual phase, a designer often only needs  
61 approximate estimations for number of different scenarios, e.g. tunnel track alternatives. To ensure  
62 a seamless workflow, the computation time should be minimised. If preliminary analysis (with  
63 consideration of uncertainties) indicates potential hazards, a more detailed evaluation of the model  
64 is required.

65 BIM has gained increasing attention in complex infrastructure projects, simplifying the planning  
66 and analysis and increasing productivity in design and construction. In tunnelling applications, the  
67 BIM concept has been used to create a tunnel information modelling framework that creates and  
68 interlinks a ground model, a tunnel lining model, a tunnel boring machine model and a built  
69 environment model [1]. Furthermore, a multi-level information representation of the built  
70 environment has been developed to support planning and analysis tasks [2]. The use of Industry  
71 Foundation Classes (IFC) enables open data exchange between several BIM software and provides  
72 a high level of compatibility [3]. The IFC standard was originally developed for the modelling of  
73 buildings and has recently been [4] extended to other fields of application in civil engineering,  
74 including bridges [5], roads [6] and tunnels [1, 7]. Nevertheless, despite 20 years of continuous  
75 development and the fact that over 200 software tools are using IFC, the interoperability issues,  
76 such as data loss and misrepresentation, are still problematic in practical projects [3].

77 As the project dimensions in tunnelling projects significantly exceed those in building projects, the  
78 concept of multi-scale modelling using several level of details (LoDs) has been proposed [8, 2].

79 Borrmann et al. [8], for example, present a comprehensive concept for incorporating multi-scale  
80 representations with shield tunnel models to efficiently link BIM with Geographical Information  
81 Systems (GIS). Their approach uses spatial IFC elements for low LoD representations and physical  
82 IFC elements for the highest LoD representations. Very recently, Abualdenien and Bormann [9]  
83 have presented an approach to support the continuous refinement of a building from the conceptual  
84 to the detailed design stages using a multi-LOD meta-model. While the purpose of this meta-model  
85 is to ensure the consistency of both the geometric and the semantic information as well as the  
86 topological coherence across different LoDs within the information model, a link to a multi-LoD  
87 numerical model is not considered.

88 As opposed to the concept of level of development (LOD), or level of model definition (LOMD),  
89 that has been introduced by the American Institute of Architects (AIA) in collaboration with the  
90 American BIMForum [10, 11], this paper refers to level of detail, LoD. According to BIMForum  
91 (2013), LoD defines how much detail is included in the model element, whereas LOD defines the  
92 degree to which the element's geometry and semantic information have been thought through in  
93 the development process. LOD, in this sense, specifies the reliability and maturity of information  
94 in the model along the design process. In summary, this paper does not focus on the model  
95 development process, but on the degree of detail that is captured for both geometry (level of  
96 geometry – LOG) and semantic information (level of information – LOI) for each of the system  
97 components.

98 In current engineering practice, the proof of tunnel design is often carried out by employing  
99 numerical simulations [12, 13, 14]. These models are usually generated based on design documents  
100 and reports. Even if the underlying information needed for numerical analysis is stored in a BIM,  
101 the translation from an information model to a computational model is still dominated by manual  
102 work. Such an approach therefore incurs significant effort carried out by experts, and is furthermore  
103 susceptible to human error. Hence, it is evident that an automated link between information  
104 management (in the form of a BIM) and numerical analysis is necessary. Such a link will enable  
105 the continuous, error-free exchange of information between BIM and numerical simulation for the  
106 stages of design, construction, and operation of a project.

107 In the field of structural analysis, the link between information and numerical models has been  
108 recently addressed in [15, 16, 17, 18, 19] where FE methods and Isogeometric Analysis (IGA) are  
109 applied for the assessment of the structural behaviour. In tunnelling application, the first attempt of  
110 linking BIM and structural assessment by means of numerical modelling is presented in [20, 21,  
111 22], where data obtained from a Tunnel Information Model (TIM) [23] is used for the automated

112 generation of a numerical model for a real-world tunnelling project, the Wehrhahn metro line in  
113 Dusseldorf.

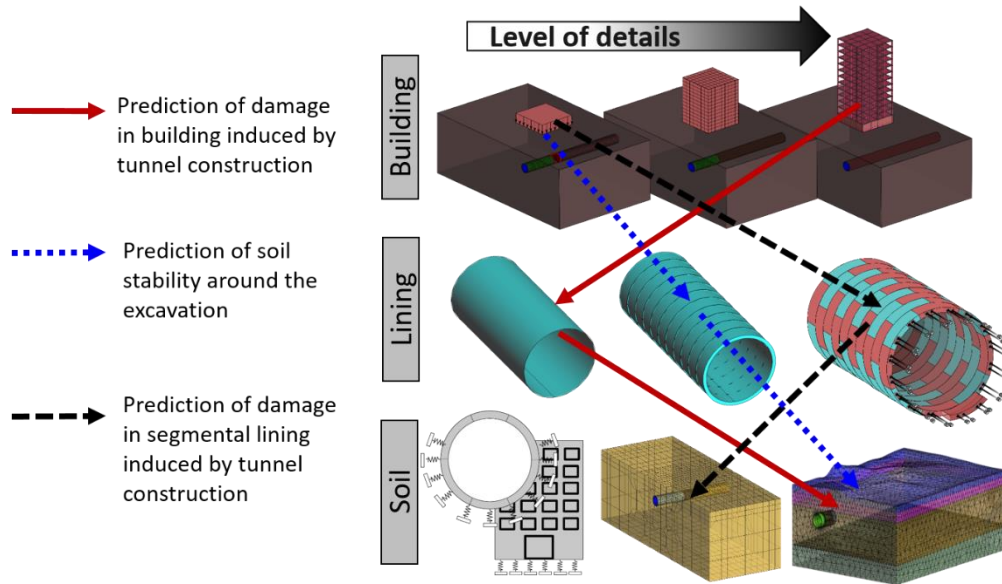
114 Based on the above, it can be stated that there have been several successful attempts to (1)  
115 demonstrate the need of a multi-LoD information model, and (2) automate the link from an  
116 information model to a numerical model at one particular LoD. What is still missing is the link  
117 between, or integration of, a multi-LoD information model and a corresponding multi-LoD  
118 numerical model. As mentioned before, this link is required to ensure a seamless design-assessment  
119 workflow, with optimised modelling and computation time, for certain design stages. For this  
120 reason, this paper presents a concept for Simulations for multi-level Analysis of interactions in  
121 Tunnelling based on the Building Information Modelling technology “SATBIM”. This forms the  
122 basis for multi-level structural analysis of the settlement behaviour [24]. To this end, parametric  
123 representations for each of the system components (tunnel lining with grouting, soil with  
124 excavation, existing buildings, and tunnel boring machine (TBM)) are developed for three different  
125 Levels of Detail.

126 This parametric information model is then used to automatically generate numerical models to  
127 simulate the tunnel construction process taking into account appropriate LoDs per component and  
128 dependent on the current design objective. Finally, the integration of multiple LoD configurations  
129 into a single IFC file is implemented for each component to enable reusability of the model in the  
130 context of BIM. The proposed concept is implemented using Autodesk Revit and Dynamo, [25],  
131 and tested in a what-if scenario analysis for a small tunnelling project.

## 132 **2. METHODOLOGY**

### 133 **2.1 Parametric multi-level modelling in urban tunnelling**

134 The main idea of the SATBIM concept is to dynamically generate simulation models from a multi-  
135 level information model at the required LoD for the specific problem to be solved. For example,  
136 minimising the overall risk of damage to buildings induced by tunnelling needs high LoD for  
137 structures and topology of the soil, however for the lining structure and its installation process, a  
138 lower LoD is sufficient to achieve high accuracy of the solution (see Fig. 1, red arrows). For the  
139 assessment of the stability of the excavated soil, high LoD is required for the soil representation,  
140 medium for the lining structure, while the building can be represented at the low LoD, e.g.  
141 surcharge load (see Fig. 1, blue dotted arrows). On the other hand, estimating stresses in the tunnel  
142 structure needs low LoD for buildings and high LoD for lining and its installation process, while  
143 surface topology of the soil is not necessary for the accuracy of the results (see Fig. 1, black dashed  
144 arrows).



145

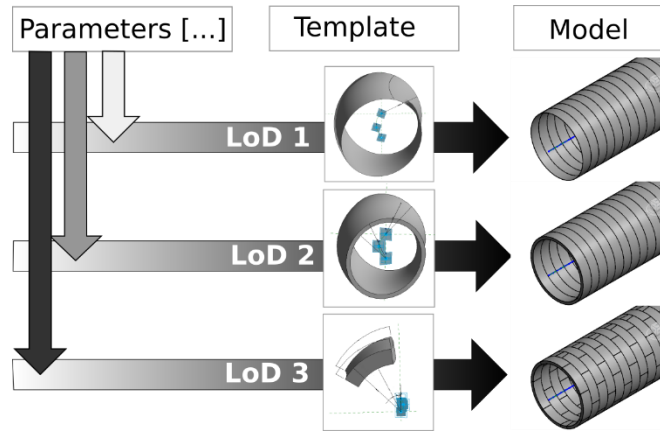
146 Figure 1: Alternatives for selection of LoDs for individual components based on the objective of  
 147 the analysis

148 The shield-supported tunnel advance beneath groundwater table in soft soil requires permanent  
 149 support of the surrounding underground to prevent the groundwater from flowing into the  
 150 construction site. A realistic model to be applied during the design and construction phase has to  
 151 represent all components of the tunnelling process relevant for the prognosis of the response of the  
 152 surrounding soil during excavation. These components include:

- 153
- soil and excavation domain,
  - 154 • segmental lining with the support measures applied at the tunnel face and at the tail void,
  - 155 • tunnel boring machine (TBM), and
  - 156 • existing infrastructure.

157 For each component three LoDs are defined: low (LoD 1), medium (LoD 2) and high (LoD 3). In  
 158 general, the LoD 1 has no volumetric representation of the components, since in the corresponding  
 159 numerical model, components are not represented with structural models but instead with the  
 160 analytical or empirical models assigned through a set of boundary conditions. The medium LoD  
 161 defines for each component a volumetric representation, where the component is “occupying” the  
 162 exact volume; however the geometry is simplified. Finally, the highest LoD includes more detail  
 163 about the actual geometry of the component. However, components such as TBM still do not  
 164 include details of the machinery and the equipment inside the shield, and therefore, an even higher  
 165 representation (LoD 4) could be introduced as an extension.

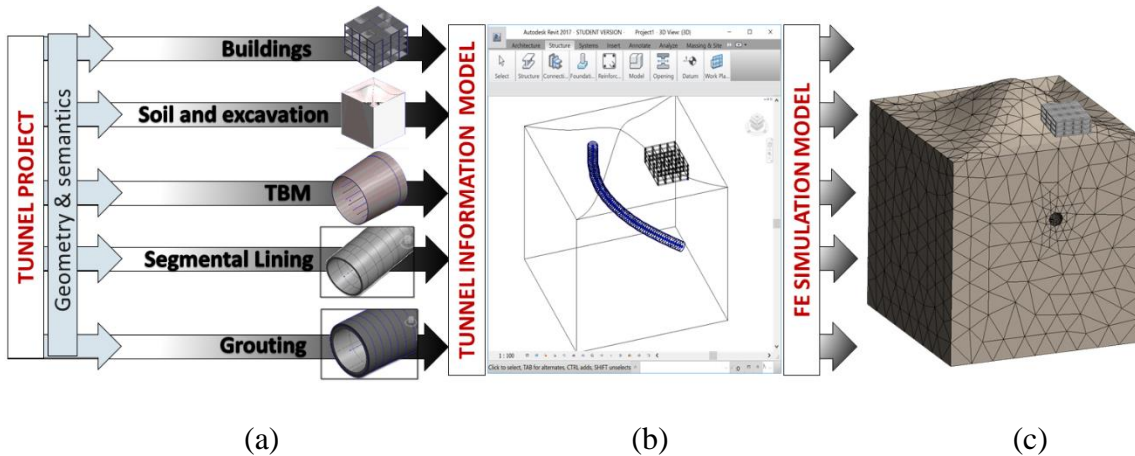
166 For each component and each LoD, a template of the corresponding component is defined. In order  
 167 to keep consistency between different LoDs, parametric consistency is defined as shown in Fig. 2.  
 168 The full set of parameters defining a component is needed for the definition of the highest LoD  
 169 (LoD 3), while only a subset of the same list is used for the definitions of medium and lower LoD  
 170 (LoD 2, LoD 1), respectively.



171

172 Figure 2: Parametric multi-level modelling: parametric consistency between different LoDs for  
 173 individual components.

174 Combining all selected components at the selected LoDs (lining with its alignment and grouting,  
 175 soil with excavation, TBM, and buildings), the complete tunnel information model is generated as  
 176 shown in Figure 3. For each component, individual local parameters (LoD, geometrical and  
 177 material parameters) are defined. On the other hand, there are also global parameters that are shared  
 178 by multiple components such as ring length, excavation radius, number of steps/slices, overburden,  
 179 etc. Further extensions for the multi-level representation of parametric components in the IFC  
 180 format are presented in Section 2.6.



181

182

(a)

(b)

(c)

183 Figure 3: Multi-level tunnel information and numerical modelling. (a) Combining sub-models  
184 based on local and global parameters. (b) Integrated tunnel information model. (c) Generated  
185 numerical model

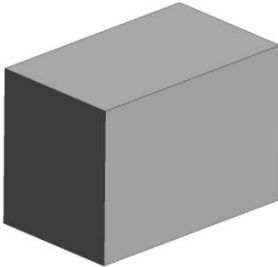
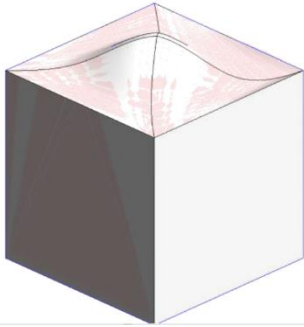
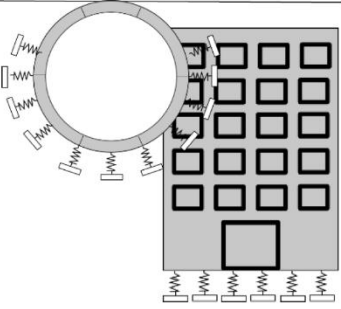
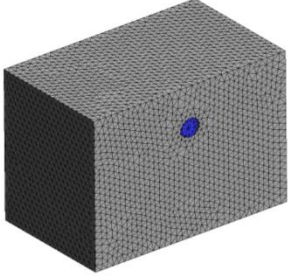
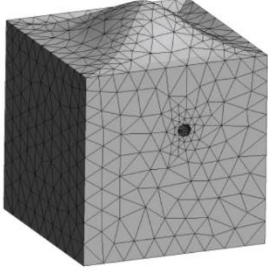
## 186 **2.2 Modelling of the soil**

187 Tunnelling projects are often characterised by complex geological conditions, where the  
188 construction is conducted through different, non-homogeneous geological layers under the ground  
189 water level. A ground model is developed based on ground investigations using boreholes and trial  
190 pits, commonly complemented by in situ testing and geophysical surveys, as appropriate to local  
191 needs and circumstances. Nowadays, tunnel project data including geotechnical information  
192 (geometry, topology, and attribute information such as groundwater data, associated geotechnical  
193 parameters, etc.) is stored either in 3D Geographic Information System (GIS) models [26, 27] or  
194 Geo Building Information Models (GeoBIM) [28]. GeoBIM has been developed to not only enable  
195 the management of subsurface construction, but also to support geo-related (subsurface) data, such  
196 as geological, hydro-geological and geotechnical objects and properties [28].

197 In numerical simulations of the mechanised tunnelling process, one of the most important  
198 requirements is the proper modelling of the soil behaviour, including complex hydraulic conditions.  
199 In relatively simple numerical models for the soil-structure interactions in tunnelling, the soil is  
200 represented by a set of boundary conditions. This is the case in the subgrade reaction model for the  
201 analysis of tunnel lining [29, 30] or the modelling of buildings with, for example, the Limiting  
202 Tensile Strain Method (LTSM) [31] or the Winkler beam method. For a more detailed  
203 representation of the tunnel construction with soil excavation, an explicit soil model with proper  
204 constitutive framework for the description of the hydraulic behaviour of the soil, as well as a  
205 realistic description of the material (stress-strain) response of the soil skeleton, is required.

### 206 **2.2.1 Geometrical and numerical modelling**

207 In terms of geometric and physical modelling of the soil, SATBIM approach offers all previously  
208 mentioned modelling variants, from simple representation of the soil with sets of boundary  
209 conditions to models considering multi-phase composition of the soil as well as accurate  
210 geometrical representation.

	LOD 1	LOD 2	LOD 3
Information model	<pre> 1 material soil_1 2 model_type drucker_prager 3 youngs_modulus 20000000.0 4 poisson_ratio 0.25 5 density 1732.0 6 porosity 0.4 7 cohesion 200000.0 8 hardening_modulus 2033333.0 9 internal_friction_angle 30.0 10 K0 1.0 11 permeability 1e-02 12 material soil_2 13 model_type drucker_prager 14 youngs_modulus 100000000.0 15 poisson_ratio 0.25 16 density 2038.0 17 porosity 0.25 18 cohesion 200000.0 19 hardening_modulus 50000000.0 20 internal_friction_angle 35.0 21 K0 1.0 22 permeability 1e-02 23 </pre>		
Numerical model			

211 Figure 4: Representation of the soil in information and numerical models on different LoDs.

212 **Soil LoD 1.** For the representation of the soil, a subgrade reaction model is adopted, where the soil  
213 is represented by infinitely thin, uncoupled springs neglecting the soil-structure interaction and the  
214 weight of the excavated soil (Fig. 4, LoD 1). The linear elastic subgrade reaction is obtained if the  
215 springs are linear ( $p = K_s \cdot u$ ), where  $p$  is the pressure between the structure and the soil,  $K_s$  is  
216 the subgrade reaction modulus, and  $u$  is the deformation. The subgrade reaction approach permits  
217 the development of elegant analytical solutions for determining the deformation of buildings, using  
218 the Winkler equation:

219 
$$EI \frac{\partial^4 w}{\partial x^4} = q_0(x) - r(x) \text{ where } r(x) = B \cdot K_h \cdot w(x) \quad (1)$$

220 where  $EI$  is the beam stiffness,  $B$  is the beam width,  $K_h$  is the coefficient of the horizontal subgrade  
221 reaction, while  $w(x)$  and  $q_0(x)$  are the deflection of the beam and load functions, respectively.

222 However, the challenge is to determine the subgrade reaction coefficient  $K_s$ , which cannot be  
223 measured directly. In a simple model proposed in [32] this coefficient is given as:

224 
$$K_s = \frac{E_s}{B \cdot I_p (1 - \nu^2)} \quad (2)$$

225 where  $I_p$  is the shape factor of the foundation. When determining the subgrade reaction modulus of  
 226 the springs for the lining model, according to [33], the stiffness of the spring is assumed to depend  
 227 on the stiffness of the soil  $E_s$ , Poisson's ratio  $\nu$  and the radius of the tunnel lining  $r$ :

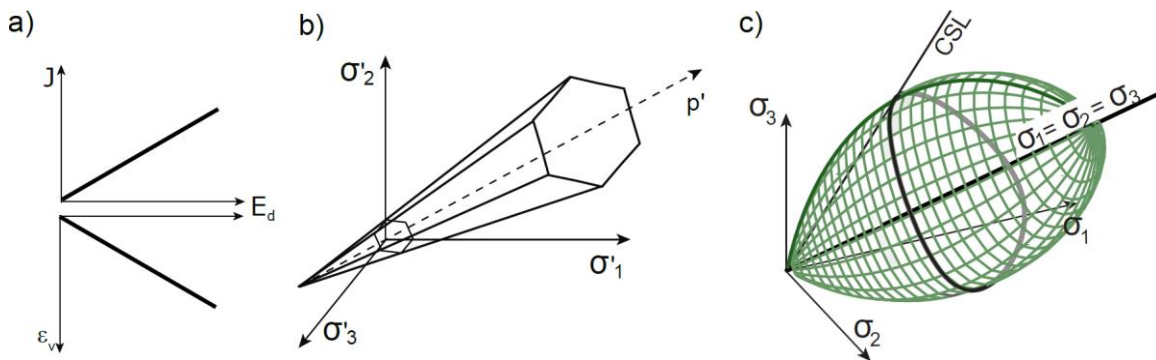
$$228 \quad K_S = \frac{E_s}{r} \frac{1-\nu}{(1+\nu)(1-2\nu)} \quad (3)$$

229 **Soil LoD 2.** In this LoD, the soil is represented by a structural finite element model, and the  
 230 geometry, determined as a bounding box, is used to delimit the simulation model. The soil is  
 231 modelled as a two-phase fully saturated material, accounting for the soil matrix and the pore water  
 232 as distinct phases according to the theory of porous media (see [34, 35] for details).

233 **Soil LoD 3.** In terms of numerical modelling, the same FE representation of the soil (two-phase  
 234 soil model for fully saturated soils) as for LoD 2 is employed here. However, the geometry is  
 235 defined using the actual CAD geometry containing soil or rock layers, their boundaries, and their  
 236 geotechnical properties in a standard format for tunnel ground models as shown in Figure 4.  
 237 Therefore, for the representation of individual layers, distinct volumes are available, and hence  
 238 distinct FE meshes are generated. In future extensions, interface conditions can be assigned  
 239 between distinct soil layers to model interactions, sliding and redistribution of pore water pressures  
 240 on the soil layer interfaces.

### 241 2.2.2 Material modelling

242 Besides establishing a proper constitutive framework for the description of the hydraulic behaviour  
 243 of the soil, a key feature of a model for tunnelling is a realistic description of the material (stress-  
 244 strain) response of the soil skeleton.



245 Figure 5: Examples for soil material models on different LoDs: a) LoD 1: Linear elastic model  
 246 (Young modulus  $E$ , volumetric strain  $\varepsilon_v$ , deviatoric stress invariant  $J$ ); b) LoD 2: Mohr Coulomb  
 247 Model; c) LoD 3: Yield surface of CASM in principal stress state and in the  $p'$ - $q$  plane [36].

248 Depending on the type of the soil and available material testing for model calibration, different  
249 material models can be applied. If there is no knowledge about the material behaviour, the simplest  
250 soil model which can be applied is a linear-elastic model (LoD 1). Since elastic behaviour is  
251 unrealistic for soils, different elasto-plastic constitutive models are available in KRATOS: the Mohr  
252 Coulomb and the Drucker Prager models, which are preferably used for sandy soils (LoD 2); and  
253 the more general Clay and Sand Model (CASM), characterised by non-associative plasticity and  
254 Lode-angle dependent yield surfaces [36], which is well suited for clayey soil (LoD 3) (see Figure  
255 5).

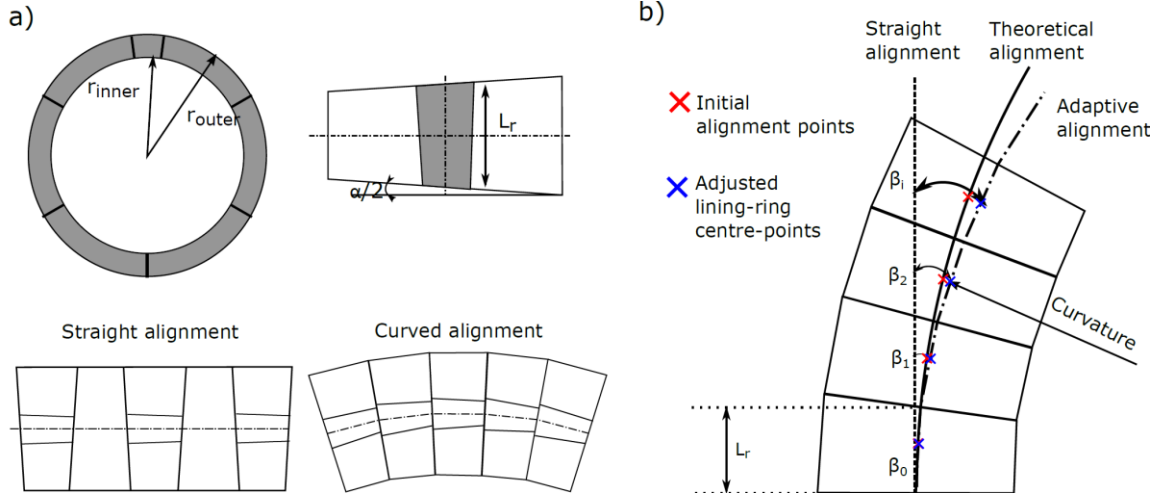
### 256 **2.3 Modelling of the segmental lining**

257 The application of segmental lining as the final tunnel support and lining is a worldwide standard  
258 for shield tunnelling technology [37] as it fulfils the main construction requirements: i) to ensure  
259 the tunnel stability behind the shield; ii) enable short installation times and iii) provide abutment  
260 for the hydraulic jacks.

261 Each tunnel project has special lining requirements, depending on the diameter, soil conditions and  
262 alignment to guarantee a safe and durable tunnel structure for an expected lifetime of 100 years or  
263 more. In order to allow for a high modularity and efficient procedures for the production and  
264 logistics of the linings, the solution that is often adopted is to employ universal rings (see Fig. 6a).  
265 In most cases, the universal segment ring is made of several segments of the same size and of one  
266 smaller segment - the key-stone - closing the ring. The universal ring is characterised by an average  
267 ring length  $L_r$ , inner and outer radius of the ring ( $r_{inner}$  and  $r_{outer}$ ), an angle describing the tapered  
268 geometry of the ring  $\alpha$ , and the number of segments and their sequence within the ring.

#### 269 **2.3.1 Alignment**

270 The designed alignment of the tunnel is accomplished by adjusting the rotations of the rings as  
271 shown in Fig 6a. For the curved parts, the rings are placed by lining up the key segments; for  
272 straight parts the rings are switched from upward key to downward key. The relative positioning  
273 of keys can be varied to modify the curved radius. The curvature of the alignment that can be  
274 achieved, given the geometry of the universal ring and the design theoretical alignment, is shown  
275 in Fig. 6b. Even though the final rotation of the ring will be determined dynamically during the  
276 tunnel construction to follow the TBM, in this paper, we developed an algorithm that determines  
277 these ring positions based on the initial design path. This is so to mimic reality and provide the best  
278 assessment of the design, taking into account the fact that ring rotations significantly affect the  
279 structural behaviour [38].



280 Figure 6: Forming the tunnel alignment based on the universal ring geometry: a) tapered  
 281 geometry of universal ring (6+1); b) design alignment vs. adaptive alignment from appropriate  
 282 rotations of ring segments

283 An algorithm for the calculation of the adaptive alignment has been developed. Based on the set of  
 284 initial lining-ring centre-points and parameters  $L_r$  (ring length),  $\alpha$  (ring continuity) and  $\theta$  (rotation  
 285 in ring plane), a new adjusted list of lining-ring centre-points is created by determining the rotation  
 286 of the lining ring such that the centre-point of the adjusted lining-ring has minimal distance from  
 287 the initial centre-points. As an output, a list of adjusted lining-ring centre-points (*list points*) and a  
 288 list of locations of ring rotations in the plane normal to the alignment (*ring rotations*) are stored.  
 289 The number of possible rotations in plane and, consequently, the angle  $\Delta\theta$  depends on the number  
 290 of segments and position of joints. There are alternatives in the ring installation strategy, such that,  
 291 for instance, the next ring can be turned only for one  $\Delta\theta$  clockwise or anti-clockwise, or  
 292 alternatively it can be turned in any of possible rotation in the plane. Regardless of the ring rotation  
 293 strategy, for any 3D design alignment, it is possible to determine the adjusted alignment following  
 294 the geometrical transformation outlined below. Starting with an initial ring and its centreline  
 295 coordinate  $x_{n-1}, y_{n-1}, z_{n-1}$ , and adding a new ring, we move to the new alignment point by a certain  
 296 differential displacement

$$297 \quad x_n = x_{n-1} + \Delta x_n \quad y_n = y_{n-1} + \Delta y_n \quad z_n = z_{n-1} + \Delta z_n \quad (4)$$

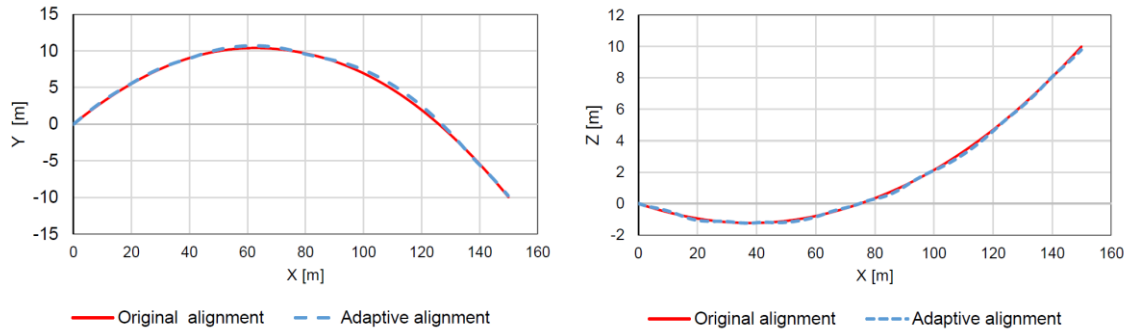
298 This differential displacement depends on the geometrical properties  $L_r$  and  $\alpha$ , as well as the rotation  
 299  $\theta$  of the ring in the ring plane as follows

$$\begin{aligned}
300 \quad \Delta x_n &= L_r \cdot \cos\left(\beta_{n-1} + \frac{\alpha}{2} \cdot \cos(\theta_{n-1}) + \frac{\alpha}{2} \cdot \cos(\theta_n)\right) \\
301 \quad &\quad \cdot \cos\left(\gamma_{n-1} + \frac{\alpha}{2} \cdot \sin(\theta_{n-1}) + \frac{\alpha}{2} \cdot \sin(\theta_n)\right), \\
302 \quad \Delta y_n &= L_r \cdot \sin\left(\beta_{n-1} + \frac{\alpha}{2} \cdot \cos(\theta_{n-1}) + \frac{\alpha}{2} \cdot \cos(\theta_n)\right) \\
303 \quad &\quad \cdot \cos\left(\gamma_{n-1} + \frac{\alpha}{2} \cdot \sin(\theta_{n-1}) + \frac{\alpha}{2} \cdot \sin(\theta_n)\right), \\
304 \quad \Delta z_n &= L_r \cdot \cos\left(\beta_{n-1} + \frac{\alpha}{2} \cdot \cos(\theta_{n-1}) + \frac{\alpha}{2} \cdot \cos(\theta_n)\right) \\
305 \quad &\quad \cdot \sin\left(\gamma_{n-1} + \frac{\alpha}{2} \cdot \sin(\theta_{n-1}) + \frac{\alpha}{2} \cdot \sin(\theta_n)\right) \tag{5}
\end{aligned}$$

306 We obtain the new inclination of the ring in the global coordinate system (in the XY plane  $\beta$  and  
307 the YZ plane  $\gamma$ ) as

$$\begin{aligned}
308 \quad \beta_{n+1} &= \beta_n + \frac{\alpha}{2} \cdot \cos(\theta_{n-1}) + \frac{\alpha}{2} \cdot \cos(\theta_n), \\
309 \quad \gamma_{n+1} &= \gamma_n + \frac{\alpha}{2} \cdot \sin(\theta_{n-1}) + \frac{\alpha}{2} \cdot \sin(\theta_n) \tag{6}
\end{aligned}$$

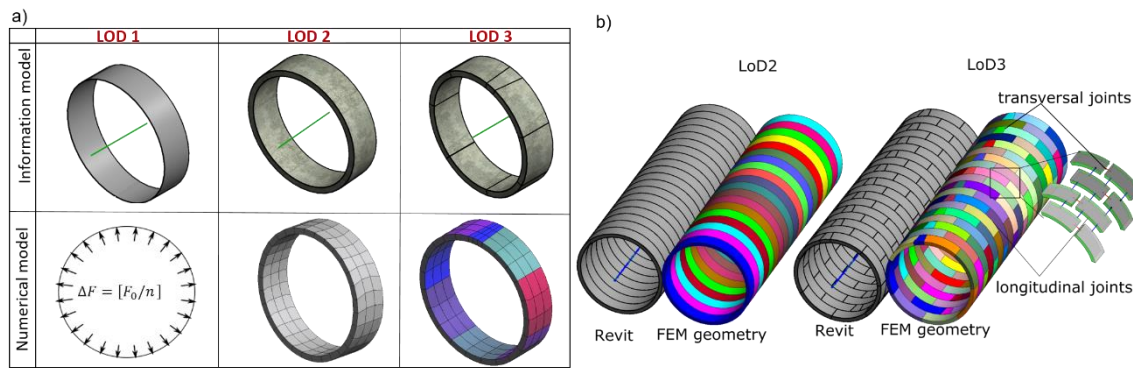
310 The algorithm initialises the lining-ring centre-points of the design alignment, and searches for the  
311 rotation in the normal plane  $\theta$  such that the deviation of the next centre point from the design path  
312 is minimised. Our implementation allows any tunnel path in 3D space to be achieved using only  
313 one universal ring. The agreement between the designed and the adapted tunnel alignment for one  
314 arbitrary case is shown in Figure 7.



315 Figure 7: Comparison between designed alignment and computed adapted alignment based on  
316 universal ring in 3D in the a) XY plane, b) XZ plane.

317 A numerical analysis of the influence of the joints of the segmental lining on the overall behaviour  
318 of the tunnel structure is typically performed without consideration of the complete tunnel  
319 construction analysis, but rather by applying sophisticated models for lining and joints, and

320 observing the behaviour under design loads, while the resistance of the soil is modelled by subgrade  
 321 reaction springs [29]. On the other hand, most sophisticated 3D simulation models for mechanised  
 322 tunnelling do not consider the segment-wise installation of tunnel lining and joints between  
 323 segments. Instead, lining is modelled using linear-elastic solid or shell elements, where the  
 324 complete lining rings are installed stepwise [39, 40, 41] . Recently, a 3D numerical models for the  
 325 shield tunnelling process was developed, where the influence of the joint pattern of the lining for  
 326 both segment joints and ring joints is taken into consideration [13]. This study has shown that the  
 327 position and stiffness of the joints have significant effects on the bending moment and normal  
 328 forces in the lining, while the effect of the joint pattern on the surface settlement is insignificant.  
 329 In the SATBIM concept, an alternative for modelling of tunnel lining is implemented, as described  
 330 below, using the multi-level approach.



331  
 332 Figure 8: Lining information and numerical models on different LoDs, b) details of the geometry  
 333 of the lining model on LoD 2 and LoD 3.

### 334 2.3.2 Geometrical modelling

335 **Lining LoD 1.** At the lowest LoD, the effect of the confinement and support provided by the lining  
 336 structure on shield tunnelling is accounted for without explicit modelling of the lining structure.  
 337 This is done by implementing the volume loss method, describing the confinement with the volume  
 338 loss coefficient  $V_l = \frac{(V_0 - V_{def})}{V_0}$  . In this method, the volume loss resulting from the completion of  
 339 excavation is prescribed together with the TBM passage (see Fig. 8a). The injection process and  
 340 the grout consolidation phase are represented by applying the change in diameter of the excavation  
 341 boundary. The method assumes that the support pressure at the tunnel boundary is reduced in  
 342 increments, and the generated volume loss can be monitored.

343 In the implemented approach, the tunnel wall is allowed to move freely and is not controlled by  
 344 confinement forces or prescribed displacements. Instead, after the de-confinement, the deformed

345 area of the tunnel is continuously calculated in each computation cycle during the displacement of  
346 the tunnel boundary. The deformations of the excavation boundaries are fixed when the volume  
347 loss value of the tunnel boundary is reached [42].

348 **Lining LoD 2.** The lining tube is modelled by means of volume elements that are activated during  
349 the simulated tunnel advance. Each lining ring is imported as a single volume, however, discretised  
350 by linear hexahedral finite elements (see Fig. 8 LoD 2). When simulating the tunnel advance, each  
351 lining ring is activated in a stress-free manner. This initialisation procedure is used to reset the  
352 reference configuration of the element. The new reference configuration of the re-activated element  
353 then matches the deformed state of the former structure.

354 **Lining LoD 3.** In order to account for the reduced stiffness of the tunnel lining due to the presence  
355 of joints and for the segment-wise installation of the tunnel lining, a model for longitudinal (ring)  
356 and transverse (segment) joints is proposed in the simulation model. Longitudinal and  
357 circumferential joints, are modelled in a discrete manner. The reduced stiffness of segmental lining  
358 ring due to the presence of joints is modelled by introducing bolts represented by beam elements  
359 and a surface-to-surface normal contact condition between segments and transversal joins of the  
360 lining rings, see Fig. 8b LoD 3. Bolts are embedded in the solid matrix representing the lining  
361 segments, where tying conditions are imposed between the integration points of the beam elements  
362 and control points in the solid segment elements with the same global coordinates. An additional  
363 normal contact condition between the facing surfaces of the segments in longitudinal and transverse  
364 direction prevents the penetration of one volume into another.

365 **Grouting.** The tail void grouting has a considerable effect on the changes of the initial stress state  
366 of the soil around the tail, which finally causes surface settlements. In particular, the re-distribution  
367 of the grouting mortar within the annular gap and the transition from liquid mortar, in the beginning,  
368 to solid state, after its hydration, plays a crucial role in maintaining the stress state of the  
369 surrounding soil and controlling the induced settlements. Therefore, in our simulation model, a  
370 constitutive model is applied that accounts for the time-dependent material behaviour of grouting  
371 mortar. Within the simulation model, the pressurization of the grouting mortar is accounted for  
372 using a two-phase formulation similar to the soil, as described in Section 2.2 for LoD 2/3. The  
373 hydration is described by time-dependent material properties for both the strength characteristics  
374 and the permeability. The formulation is based on the model for hydration of young concrete  
375 proposed in [43] and applied to grouting mortar in [44].

## 376 **2.4 Modelling of the tunnel boring machine (TBM)**

377 In shield tunnelling, the TBM is pushed forward by elongation of hydraulic jacks, and excavates  
378 the soil by a rotating cutting wheel and supports the material around the excavation area via the

379 shield skin. In terms of numerical modelling, there are different approaches of representing the  
 380 shield machine. Since the main function of the shield is to prevent that the material around the  
 381 excavation area moves into the tunnel excavation, one option is to represent the TBM simply by  
 382 boundary conditions limiting the deformation of the soil [45]. However, the TBM is also a  
 383 deformable body and the taper of the TBM and the frictional contact of the shield skin with its  
 384 surroundings play an important role for the re-distribution of stresses and pore pressures in the soil.  
 385 Therefore, the TBM can be represented using a 3D model interacting with the surrounding soil  
 386 through a frictional interface [46]. An additional advanced modelling feature is to account for the  
 387 hydraulic jacks that are attached to the TBM by using the previously erected lining segments as  
 388 thrust bearings. In order to prevent divergence of the machine from the alignment, the thrust jacks  
 389 are also used to steer the shield by setting different jack pressures [18].

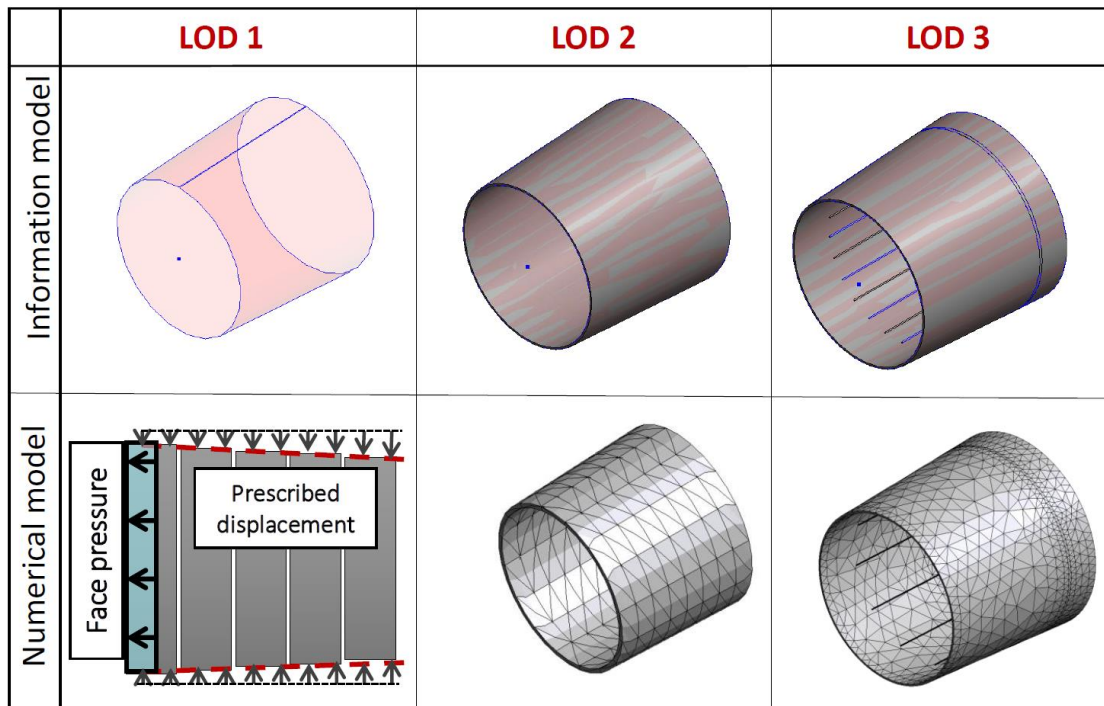


Figure 9: Information and numerical modelling of the TBM on different LoDs.

390

391

392 **TBM LoD 1.** To model the TBM as an obstacle for limiting the deformation of the soil, the shield  
 393 is represented by boundary conditions [45], as illustrated in Figure 9. In this approach, the shield is  
 394 represented by a set of  $n$  segments with length  $L_r$  with uniformly defined boundaries in terms of  
 395 radial displacements that approximate the conical surface of the shield, where  $n = L_{TBM} / L_r$  and  
 396  $L_{TBM}$  is the total length of the machine.

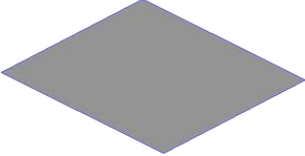
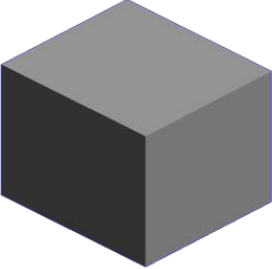
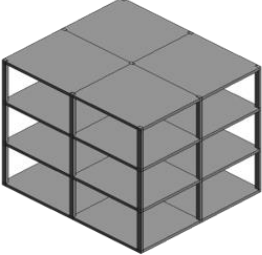
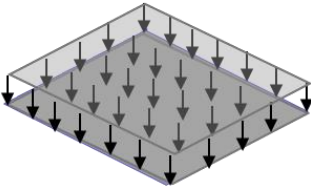
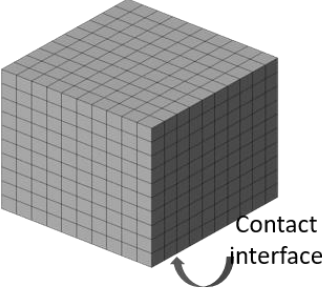
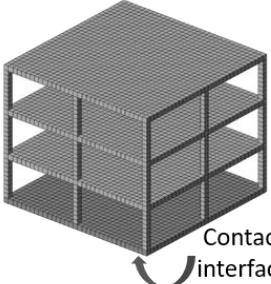
397 **TBM LoD 2.** The TBM is modelled as a deformable body moving through the soil and interacting  
 398 with the ground using surface-to-surface contact. By virtue of this modelling approach, the volume

399 loss due to the excavation process naturally follows the real, tapered geometry and the over-cutting  
400 of the shield machine [40]. The frictional contact between the shield skin with the surroundings  
401 plays an important role in the re-distribution of stresses and pore pressures in the soil. It is therefore  
402 modelled by means of surface-to-surface contact formulation introduced by [47]. The contact  
403 formulation imposes a geometric constraint between the contacting (“slave”) body (the TBM) and  
404 the contacted (“master”) body (the soil) which controls the interaction between the two bodies with  
405 independent deformations. The displacements of the TBM are prescribed at the TBM tail, and the  
406 direction of advance is determined by the calculated tunnel alignment vector.

407 **TBM LoD 3.** The highest LoD describes the advancement of the TBM by elongation of hydraulic  
408 jacks, excavating the soil with a rotating cutting wheel. In order to realistically model the movement  
409 of the TBM and its interaction with the soil, to avoid drift off-course of the TBM and to simulate  
410 curved tunnel advances, an automatic steering algorithm, to control the individual jack thrusts  
411 similar to the one proposed in [44], is used to keep the TBM on the designed alignment path (see  
412 [18] for details). Identical to LoD 2, the interaction between the soil and TBM skin is modelled by  
413 applying frictional surface-to-surface contact conditions.

## 414 **2.5 Modelling of the existing infrastructure**

415 Tunnelling-induced settlements in urban areas are influenced by the interaction of existing  
416 structures (e.g. buildings) with the soil deformations. To consider this mutual influence, reduced  
417 models for structures are generally sufficient. However, if the objective of the analysis is to assess  
418 the effect of tunnelling on the behaviour of existing structures, detailed structural models are  
419 required. The selected LoDs for the representation of buildings are chosen such that the lowest LoD  
420 will not introduce any additional DoFs, but represent the buildings by means of additional stresses  
421 due to building weight, while the higher LoDs have a detailed representation of the building  
422 structure and include the relevant soil-structure interaction effects (see Figure 10). In the current  
423 state of development, a linear elastic material model is used for building representation, which can  
424 be used for damage detection using model updating techniques [48]. For direct estimation of a  
425 damage index, non-linear damage models are to be developed in future extensions of the  
426 framework.

	LOD 1	LOD 2	LOD 3
Information model			
Numerical model			

427 Figure 10: Information and numerical modelling of existing buildings using different LoDs

428 **Building LoD 1.** The building is substituted by a dead load from the building weight acting on the  
429 soil surface as shown in Figure 10 (LoD 1). In this model, the effect of the soil-structure interaction  
430 and building stiffness are neglected. An algorithm is implemented to search the nodes in the soil  
431 domain that corresponds to the polygon of the building footprint. A distributed building dead load  
432 is applied to this group of nodes.

433 **Building LoD 2.** Buildings are considered in the tunnelling model by means of reduced models  
434 with a substitute elastic stiffness  $E$ , height  $H$  and weight, computed according to an approach  
435 proposed in [49]. In the presented FE formulation, isotropic volume tri-linear hexahedra elements  
436 are adopted with respective structural properties, interacting with the soil through a mesh-  
437 independent surface-to-surface contact algorithm, which prevents the penetration of the foundation  
438 of the building into the soil. It also takes into account the different mechanisms of the soil-structure  
439 interaction corresponding to the “sagging” and “hogging” modes.

440 **Building LoD 3.** Buildings are modelled as full structural frame models. The columns and floors  
441 are both modelled with isotropic volume hexahedra elements. In order to control the number of  
442 DoF, a quadratic structured mesh is generated, where a user-defined parameter is assigned to  
443 control the mesh size. For a detailed assessment of the stresses induced in the structures, the  
444 appropriate mesh size should be determined based on convergence studies. Since foundations

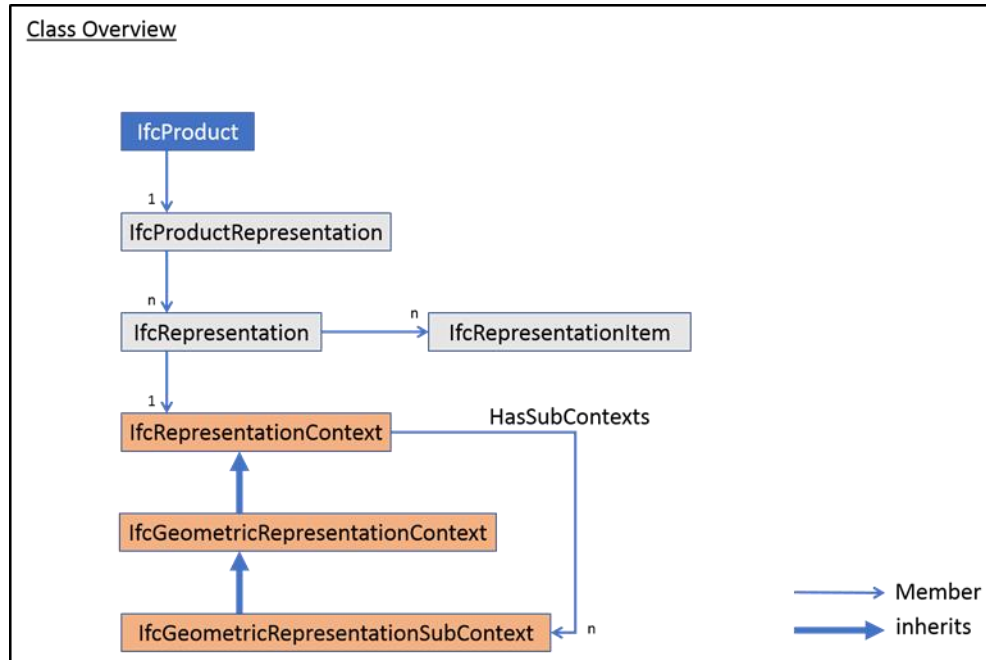
445 play a fundamental role in the transmission of the ground deformations to the building, surface-  
446 to-surface contact conditions are introduced between the soil and foundation to simulate such  
447 relative deformations,.

## 448 **2.6 Multi-level information modelling in IFC**

449 The Industry Foundation Classes (IFC) are considered as an appropriate information exchange  
450 format to support several BIM use cases throughout the facilities life-cycle, such as high-fidelity  
451 one-way design transfer, design coordination and checking among different disciplines, facility  
452 management handover, facility inspection and maintenance as well as visualisation [50]. For this  
453 reason, it makes sense to come up with a concept for representing multi-LoD information models  
454 in IFC to eventually be able to support these use cases.

455 Generally, there are two different approaches for representing geometry at different levels of detail  
456 in the Industry Foundation Classes (IFC). The first approach employs several separate IFC files for  
457 each level of detail. The second approach focuses on using different representation contexts to  
458 distinguish different levels of detail within one IFC File. Figure 11 outlines a class diagram that  
459 shows how to use such contexts. By concept, each *IfcProduct*, which includes geometrical  
460 representation, assigns an *IfcProductRepresentation*. Usually, this product representation includes  
461 exactly one *IfcRepresentation*, which defines one shape model. The actual geometric information  
462 is then assigned using one or multiple instances of *IfcRepresentationItem*. It also assigns a default  
463 *IfcGeometricRepresentationContext* that provides information about dimension, precision,  
464 coordinate system and true north. It further allows the assignment of multiple instances of  
465 *IfcGeometricRepresentationSubContext* “... to define semantically distinguished representation  
466 types for different information content ... to control the level of detail of the shape representation  
467 that is most applicable to this geometric representation context.” [43].

468 Comparing these approaches, there are advantages and limitations to each. Using separate files for  
469 representing different levels of detail does not depend on the format itself. Also, it does not require  
470 target software to support different representation contexts, but it requires the user to maintain an  
471 appropriate naming structure outside the file format and loading different level of detail manually  
472 into the target software. When considering not only geometric content, but also different sets of  
473 properties, which are assigned to separate levels of detail, using different files is error-prone.



474

475

Figure 11: UML Class Diagram of IfcRepresentationContext

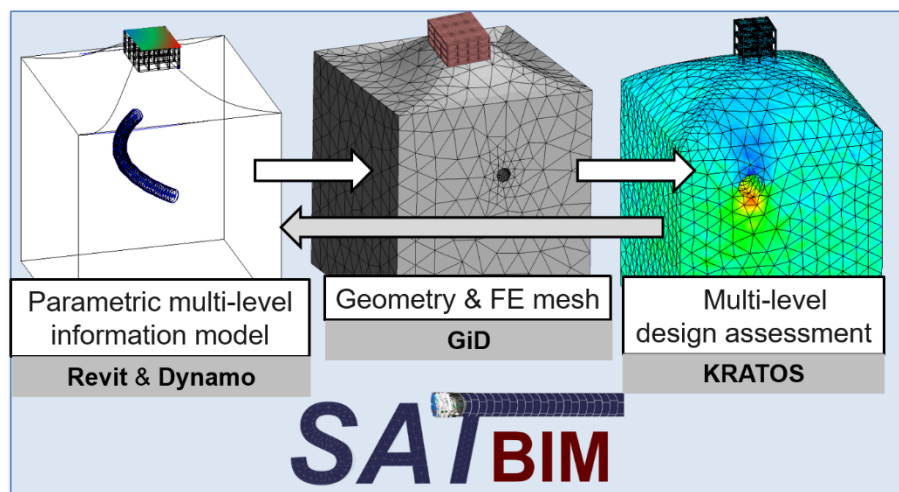
476 Using the IFC built-in concept of the *IfcRepresentationContext*, a proper decoupling between  
 477 semantic and geometry levels of detail can be implemented by concept but requires the target  
 478 software to support such contexts. This approach also allows the storing of all possible levels for  
 479 each product. However, in this case the modeller should account for not overloading the IFC  
 480 content by unnecessary levels of detail that may result in performance issues. Furthermore, this  
 481 approach only applies for the geometric content, whereas the different sets of properties cannot be  
 482 bound to a specific context. A workaround could store different sets for each level of detail, which,  
 483 for example, can be linked afterwards by using the *IfcGeometricRepresentationContext*'s value of  
 484 the attribute *UserDefinedTargetView*, like "LoD1", as an identifying prefix.

### 485 3. IMPLEMENTATION AND CASE STUDIES

#### 486 3.1 Prototype implementation

487 The multi-level information model for tunnelling is developed using the industry-standard tools  
 488 Revit and Dynamo [25], allowing for consistent parametric modelling on different LoDs. For each  
 489 tunnel component and for each LoD, a template for the corresponding component is created using  
 490 "Revit families". A family in Revit is a class with parametric definitions and constraints, allowing  
 491 the definition of specific family attributes for individual family instances (Revit objects). In order  
 492 to keep consistency between different LoDs, A parametric consistency between templates is  
 493 defined in SATBIM as shown in Figure 2 and as introduced in Sections 2.2, 2.3, 2.4, and 2.5. The  
 494 full set of parameters defining a component is needed for the definition on the highest LoD, while

495 only a subset of the parameter list is used for lower LoDs. This way of handling parameters allows  
 496 for automated preservation of the consistency of the multi-scale model.  
 497 For each model component for each LoD, a corresponding numerical model has been developed  
 498 using the pre/post processor GiD [51] and the open source Finite Element simulation software  
 499 KRATOS [52]. The generation of the complete structural model, consistency between individual  
 500 components, simulation scripts and visualisation features are handled by our newly developed  
 501 software called “SatBimModeller”. A Python routine, *MaterialPropertiesUtility*, is used to enable  
 502 a user-friendly input of the material properties. All details about the newly developed modeller can  
 503 be found in [53]. The validation of the proposed computational framework can be found in [20,  
 504 21].



505

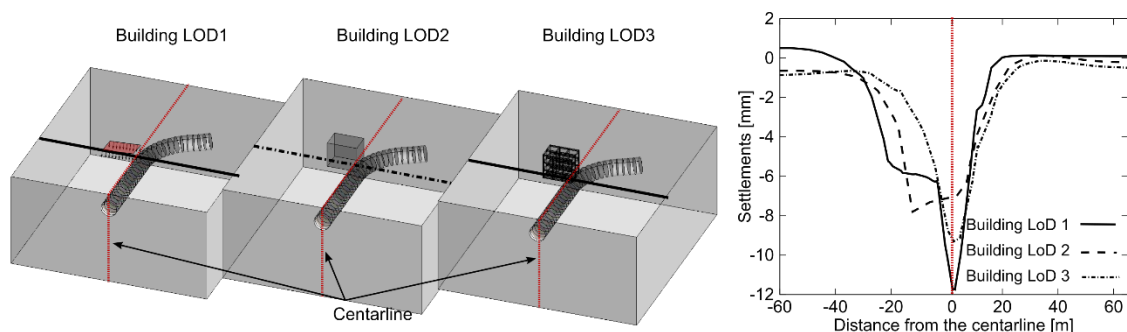
506 Figure 12: Workflow and implementation of the SATBIM framework

### 507 3.2 LoD selection for different scenarios of the analysis

508 The choice of the component LoD in both information and numerical model depends on the  
 509 scenario of the analysis and the maturity of the analysis (in earlier design stages only approximate  
 510 or relative quantities are sufficient). Higher accuracy in modelling leads to more reliable design  
 511 assessment. However, this will also incur high modelling and computational costs. Therefore, an  
 512 optimal LoD should be selected depending on the objective of the analysis and information  
 513 available at the current stage of design. The following examples will discuss different scenarios for  
 514 the selection of LoDs for the analysis of tunnelling-induced settlements and deformation of the  
 515 structure.

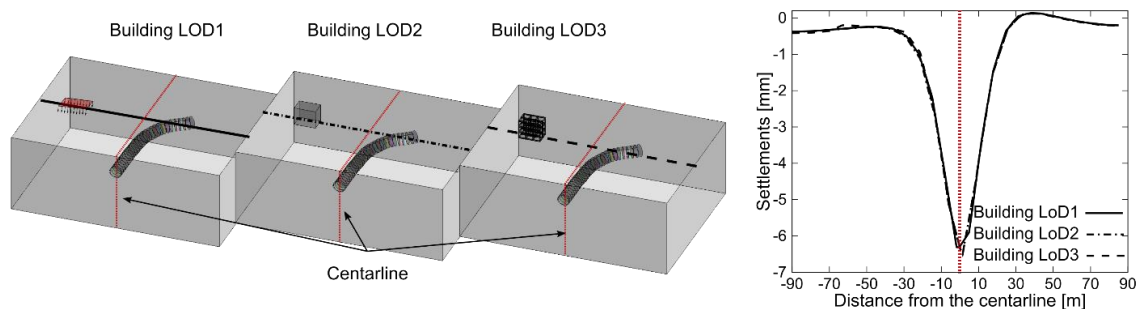
516 The first problem exemplifies the selection of the building LoD for the estimation of tunnelling-  
 517 induced settlements. In the example shown in Figure 13, a building with dimensions  $18.5\text{ m} \times$

518  $12.5\text{ m} \times 15.8\text{ m}$  (length  $\times$  width  $\times$  height) is located above a tunnel of 10 m diameter (D). The  
 519 middle axis of the building is offset from the centreline of the tunnel by 10 m (1D), and the  
 520 tunnelling-induced settlements trough is observed for a building representation at LoDs 1-3  
 521 (accounting for building weight), soil at LoD 2, lining at LoD 1 (the volume loss method, with  $V_l =$   
 522 0.5 %) and the TBM at LoD 1. The plot in Figure 13 shows the importance of the choice of the  
 523 building LoD for both settlements and structural deformation. Maximum settlements are obtained  
 524 for building LoD 1 due to the negligence of the building stiffness in soil-structure interaction. In  
 525 contrast, for building LoD 2, this interaction effect is overestimated (very stiff structural response),  
 526 compared to LoD 3, where a balance between soil and building stiffness is achieved.



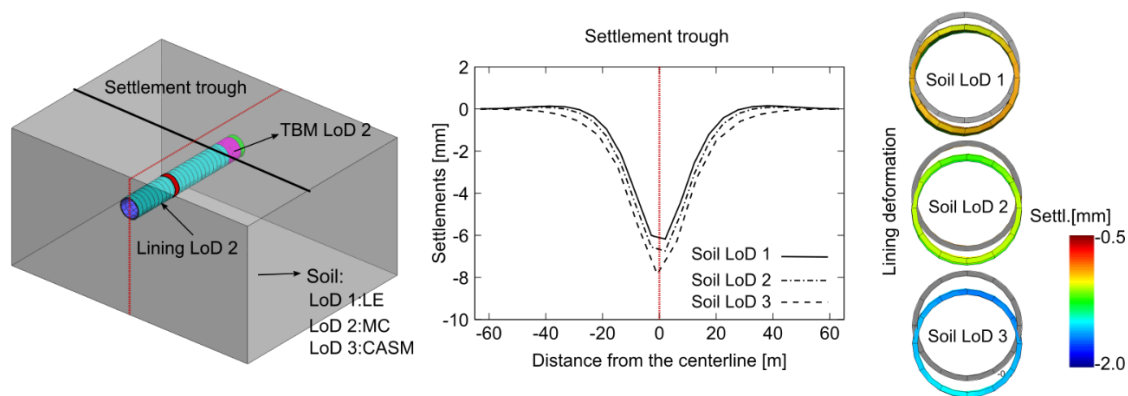
527  
 528 Figure 13: Impact of building LoD representation on tunnelling-induced settlements when the  
 529 building is above the tunnel

530 In contrast, if the building is located far from the tunnel (middle axis of the building is offset from  
 531 the centreline of the tunnel by 50 m (5D)), as shown in Figure 14, the choice of the building LoD  
 532 is irrelevant, since tunnelling-induced settlements do not depend on the building representation. A  
 533 detailed analysis of the sensitivity of building LoD representation to the building distance from the  
 534 tunnel alignment and the tunnel depth can be found in [54]. These analyses show that the LoD of  
 535 the building is irrelevant if the distance of the building from the tunnel centreline is larger than 4D.



536  
 537 Figure 14: Impact of building LoD representation on tunnelling induced settlements when the  
 538 building is far away from the tunnel

539 The second scenario investigates the effect of the selection of the soil LoD on the tunnelling-  
540 induced settlements and the deformation of the tunnel structure. In this example, lining and TBM  
541 are modelled at LoD 2, while the soil material is varied from LoD 1 (Linear Elastic model - LE),  
542 LoD 2 (Mohr Coulomb - MC) to LoD 3 (CASM) with the properties given in Table 1. From the  
543 plot shown in Figure 15, it is clear that introducing the non-linearity in soil behaviour, i.e. higher  
544 LoD, results in higher settlements. From the illustrated deformed tunnel ring, on the right side of  
545 Figure 15, it can be seen that higher settlements will cause higher vertical movement of the ring.  
546 However, the difference in ring shape is very small, because the ring moves almost as a rigid body.  
547 Therefore, the induced structural forces in all three cases are similar. Hence, if the target of analysis  
548 is the estimation of soil stability, then a higher LoD for the soil should be selected, however, the  
549 lining can be modelled at LoD 2.



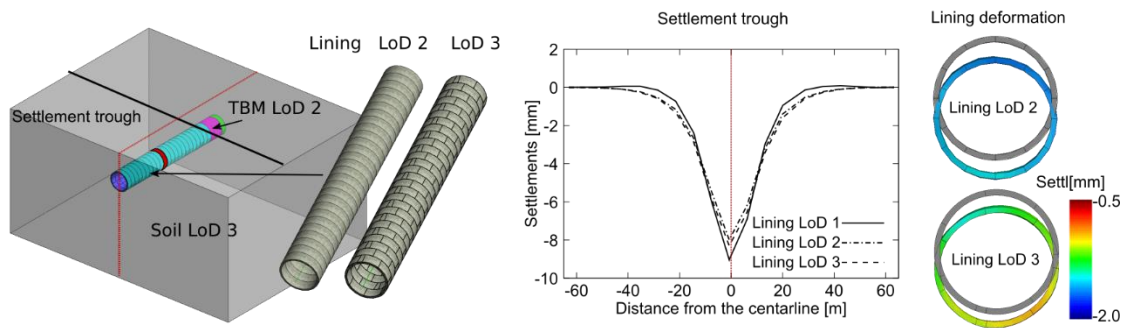
550  
551 Figure 15: Tunnelling-induced surface settlements trough and lining ring deformation for soil  
552 representation using LoD 1: LE, LoD 2: MC, and LoD 3: CASM

553 Table 1: Material parameters for the soil models for examples in Figures 14, 15, 16

Component	Soil			Lining	TBM
	LE	MC	CAS	LE	LE
Constitutive law					
Young modulus (MPa)	80	80	80	$2 \times 10^4$	$2 \times 10^5$
Poisson ratio	0.25	0.25	0.25	0.3	0.3
Density (kg/m <sup>3</sup> )	1732	1732	1732	2500	7620
Porosity	0.4	0.4	0.4	—	—
Cohesion (kPa)	—	200	—	—	—
Hardening modulus (MPa)	—	58.3	—	—	—
Friction angle (degrees)	—	30	—	—	—
Dilatancy angle (degrees)	—	30	—	—	—
Permeability (m/s)	0.00	0.00	0.001	—	—
Slope of the unload/reload curve in $(v - \ln p')$ space, $\kappa$	—	—	0.001	—	—
Slope of the normal compression curve in $(v - \ln p')$ space, $\lambda$	—	—	0.01	—	—

Spacing ratio, $r$	—	—	0.2	—	—
Shape parameter of the yield surface, $n$	—	—	2	—	—
Slope of the critical state line under triaxial compression, $M$	—	—	1.08	—	—
Initial preconsolidation mean stress for soil, $P_0$ (kN/m <sup>2</sup> )	—	—	$10^{15}$	—	—

554 The third scenario, shown in Figure 16, investigates modelling of the tunnel lining, where the same  
555 model as in scenario 2 is used in terms of geometry and modelling of TBM. The soil is modelled  
556 at LoD 3, and the tunnel lining is modelled either using the volume loss method (LoD 1), as a solid  
557 ring (LoD 2), or as a segmented ring (LoD 3). For the volume loss method (lining LoD 1), we need  
558 to predefine the volume loss coefficient, which for this example  $V_l = 0.8\%$  is used. This resulted  
559 in a slightly different settlements trough for lining LoD 1 (0.3 mm) compared to lining LoD 2 and  
560 LoD 3, which are almost identical (see Figure 16 settlement trough). However, if the deformation  
561 of the lining ring for LoD 2 and LoD 3 are compared, we can see, as seen in scenario 2, that the  
562 solid ring moves vertically as a rigid body, while the segmented ring deforms to a more oval shape,  
563 which will induce higher forces. Hence, for the estimation of surface settlements lining LoD 2 is  
564 sufficient, however, if one needs detailed insight into the structural deformation, lining LoD 3 is  
565 required.



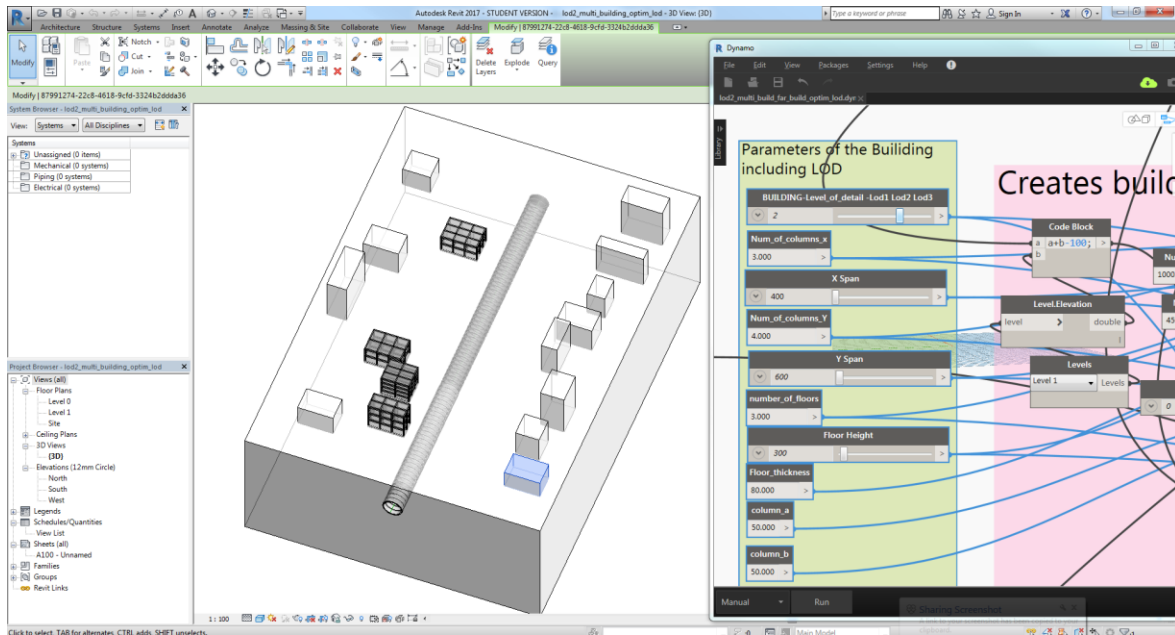
566  
567 Figure 16: Impact of lining LoD on the tunnelling-induced surface settlements trough and the  
568 lining ring deformation

569 For further details about model sizes, FE meshing and simulations setup, all models are available  
570 in the SATBIM repository at <https://github.com/satbim/satbim/>.

### 571 3.3 Multi-level simulation of a tunnelling project

572 The SATBIM platform has been successfully applied for the generation of information and  
573 numerical models and for the visualisation of structural assessment. Depending on the design  
574 scenario, the optimal LoD of each individual component is selected, leading to a robust and  
575 computationally efficient numerical assessment (see Figure 17). Knowledge about the optimal  
576 building LoD for the scenario of shield tunnelling in the vicinity of existing infrastructure, taken

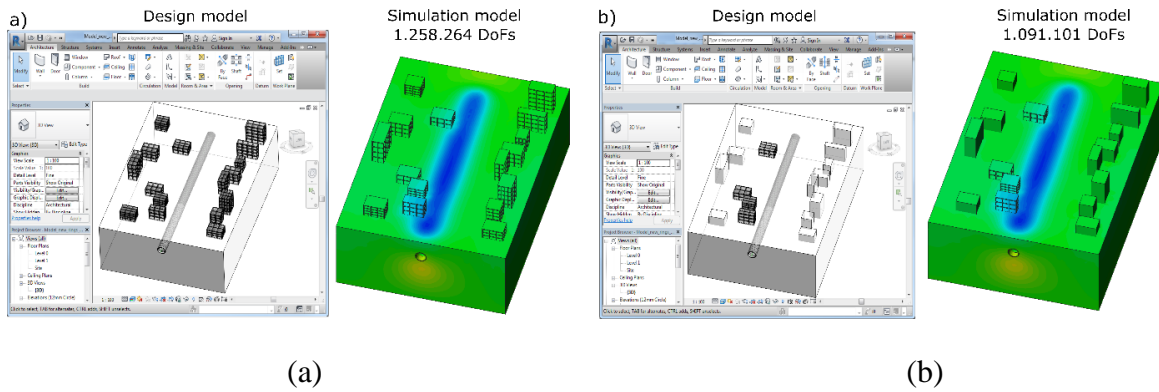
577 from previous studies conducted based on the SATBIM concept [54], is applied to further optimise  
578 the size of the model without reducing the accuracy of the solution.



579

580 Figure 17: Parametric information model for a 200 m long tunnel section in Revit and Dynamo  
581 used for the generation of a large-scale simulation. Selection of the optimal LoD of the building  
582 in Dynamo user interface.

583 In a first simulation all buildings included in the BIM model of the investigated tunnel section are  
584 modelled with the highest LoD (see Figure 18a), while in a second numerical analysis, only  
585 buildings having a high sensitivity w.r.t. the LoD are modelled with high accuracy, while the rest  
586 is modelled with LoD 2, which significantly reduces the size of the problem (see Figure 18b). In  
587 both models, LoD 2 is selected for the representation of the tunnel lining structure and the TBM.  
588 This model accounts for the shield as a deformable body moving through the soil and interacting  
589 with the ground through surface-to-surface contact. The tunnel advance is modelled by means of  
590 de-activation of soil elements and installation of the lining rings and grouting elements. Tunnelling-  
591 induced deformations are controlled by applying the face support pressure and the grouting pressure  
592 at the tunnel face and in the steering gap, respectively. The elasto-plastic Mohr Coulomb model  
593 with associative flow rule is used as the constitutive relation between effective stresses and strains  
594 in the fully saturated soil. The groundwater level is assumed at the surface. The tunnel is constructed  
595 with 80 lining rings of 2.5m length and 10m radius are excavated under 17.5m of soil overburden.  
596



597

598

599 Figure 18: Information (design) and simulation model for a more than 200m long tunnel section  
 600 used for the generation of a numerical simulation and results of FE simulation generated using  
 601 “SATBIM-Modeller” for a) Model 1: highest LoD for representation of the infrastructure and b)  
 602 Model 2: optimised LoD for representation of the infrastructure.

603 Considering a spatial discretization of all components (soil, lining, TBM and buildings) the models  
 604 are finally described with 1,258,264 and 1,091,101 Degrees of Freedom (DoFs) for Model 1- high  
 605 (LoD3) and Model 2- optimised (LoD2 and LoD3) representation of buildings, respectively.  
 606 Selecting the optimal LoD for the buildings, the model size has been reduced by 17% in terms of  
 607 number of DoFs, while keeping the accuracy of the numerical solution, as shown in Figure 18a and  
 608 b. The model size strongly influences the computational costs as shown in Table 2, where the  
 609 individual as well as the total time for the solution are listed.

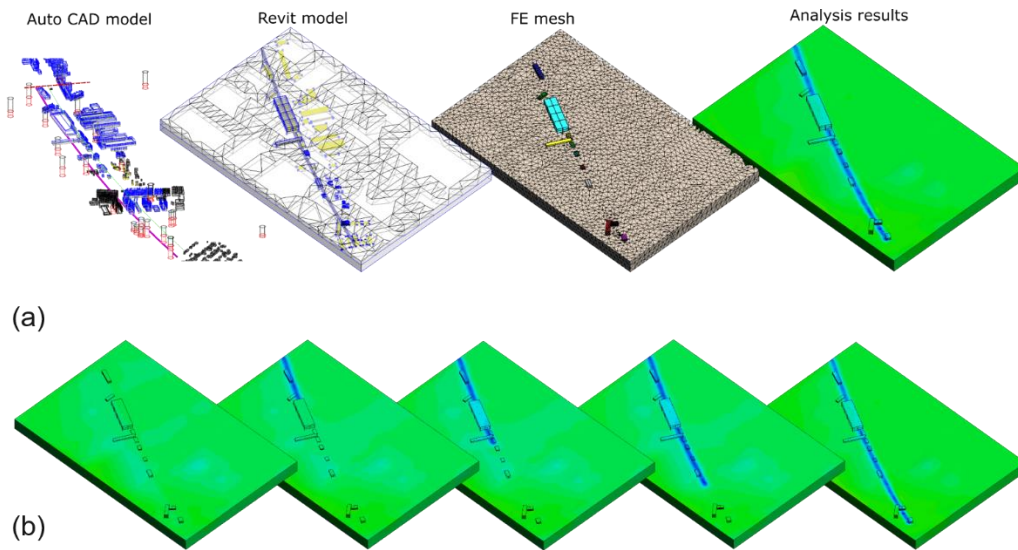
610 Table 2: Runtime for the solution steps of Model 1 and Model 2 from the Figure10.

Computational costs	Model 1 (high LoD)	Model 2 (optimised LoD)
Conditioning time per step[s]	4.2	3.6
Assembly time per step [s]	26.2	19.8
Solve time per step [s]	281.7	244.2
I/O time per step [s]	4.0	3.6
Total time [min]	2916	2410

611 Although the size of the model and consequently the computational costs differ significantly, the  
 612 final output of the numerical analysis is identical for Models 1 and 2 as shown in Figure 18. This  
 613 is due to fact that the complexity of the model is optimised without affecting the important, i.e. the

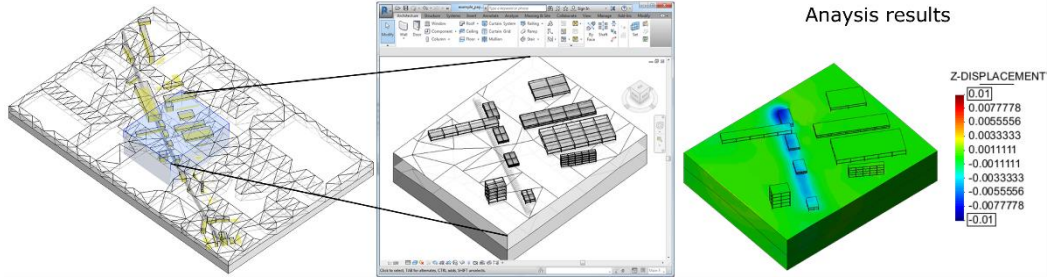
614 influencing features of the model w.r.t. the objective of the analysis, which in this case is tunnelling-  
615 induced settlements and interaction with existing buildings. Further improvement of the  
616 computational efficiency of the SATBIM framework by means of parallelisation is presented in  
617 [54].

618 The SATBIM framework has also been tested on real tunnel data including 3D topology of the  
619 ground based on borehole data, 3D tunnel alignment, and building models created based on a City  
620 model data, to create and analyse a large tunnel section of approximately 1km length. Figure 19 (a)  
621 shows how the SATBIM framework is used for a fully automatic generation of the information  
622 model based on the CAD data. The information model was further used for the generation of the  
623 simulation models and design assessment of the tunnel construction as illustrated in Figure 19 (b).  
624 Initial calculations of a large tunnel section were conducted with a low LoD for the structural  
625 components. The evolution of tunnelling-induced displacements and their effects on the existing  
626 infrastructure were evaluated as illustrated in Figure 19 (b). Secondly, for the tunnel section, where  
627 potential risks on the existing structure have been identified, a more detailed analysis was  
628 conducted, adopting higher LoDs for the structural components (lining (LoD 3), buildings (LoD 3)  
629 and TBM (LoD 2)) as illustrated in Figure 20.



630

631 Figure 19. (a) Automated workflow for design and assessment based on project data in SATBIM;  
632 (b) development of surface settlements and soil-structure interaction.



633

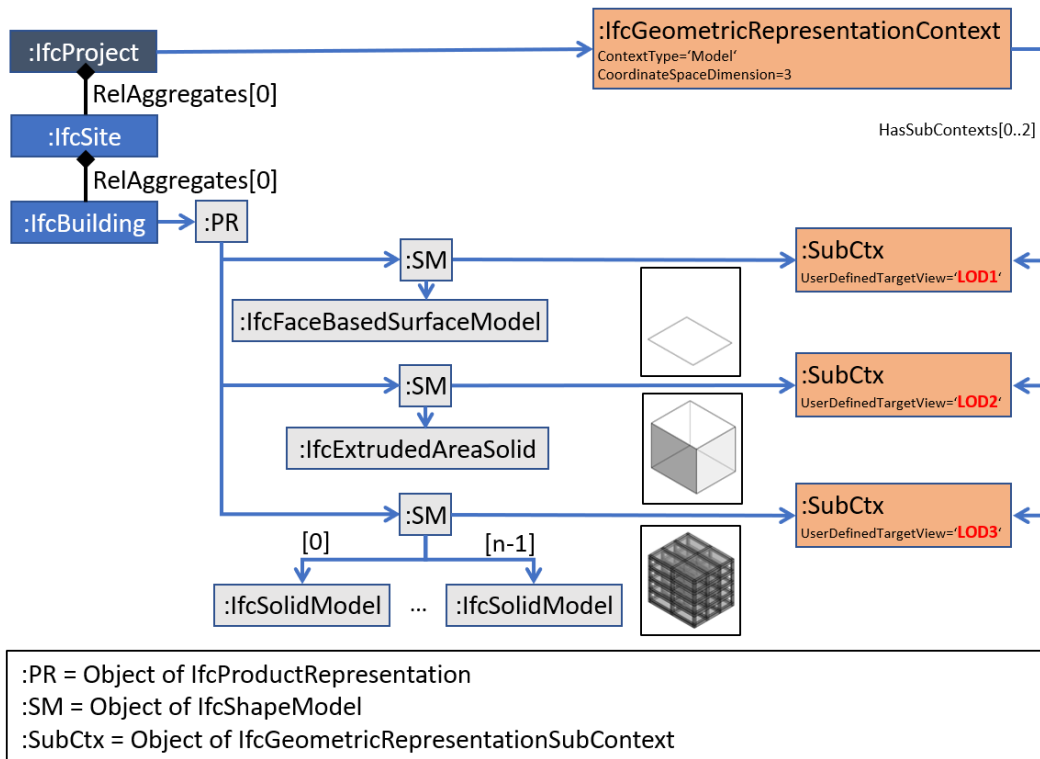
634 Figure 20. Further evaluation of critical sections considering a higher level of representation for  
 635 structural components.

### 636 3.4 Multi-level IFC representation of a tunnelling project

637 While Revit only allows the export of one single configuration of the model, where the geometry  
 638 of the domain models is fixed to a specific LoD, we developed a custom solution to implement the  
 639 suggest LoD modelling concept. To this end, we implemented the so-called Zero Touch Extension  
 640 for Dynamo, which uses the IFC Engine DLL Application Interface [55] to integrate multiple LoD  
 641 configurations into a single IFC file.

642 As the control of the representation contexts in IFC is limited to the project level, different domain  
 643 models (buildings, tunnel, TBM and ground) are still exported to separate IFC files. Moreover,  
 644 each building model of the existing infrastructure should provide different LoDs, resulting in  
 645 separate IFC files, one per building.

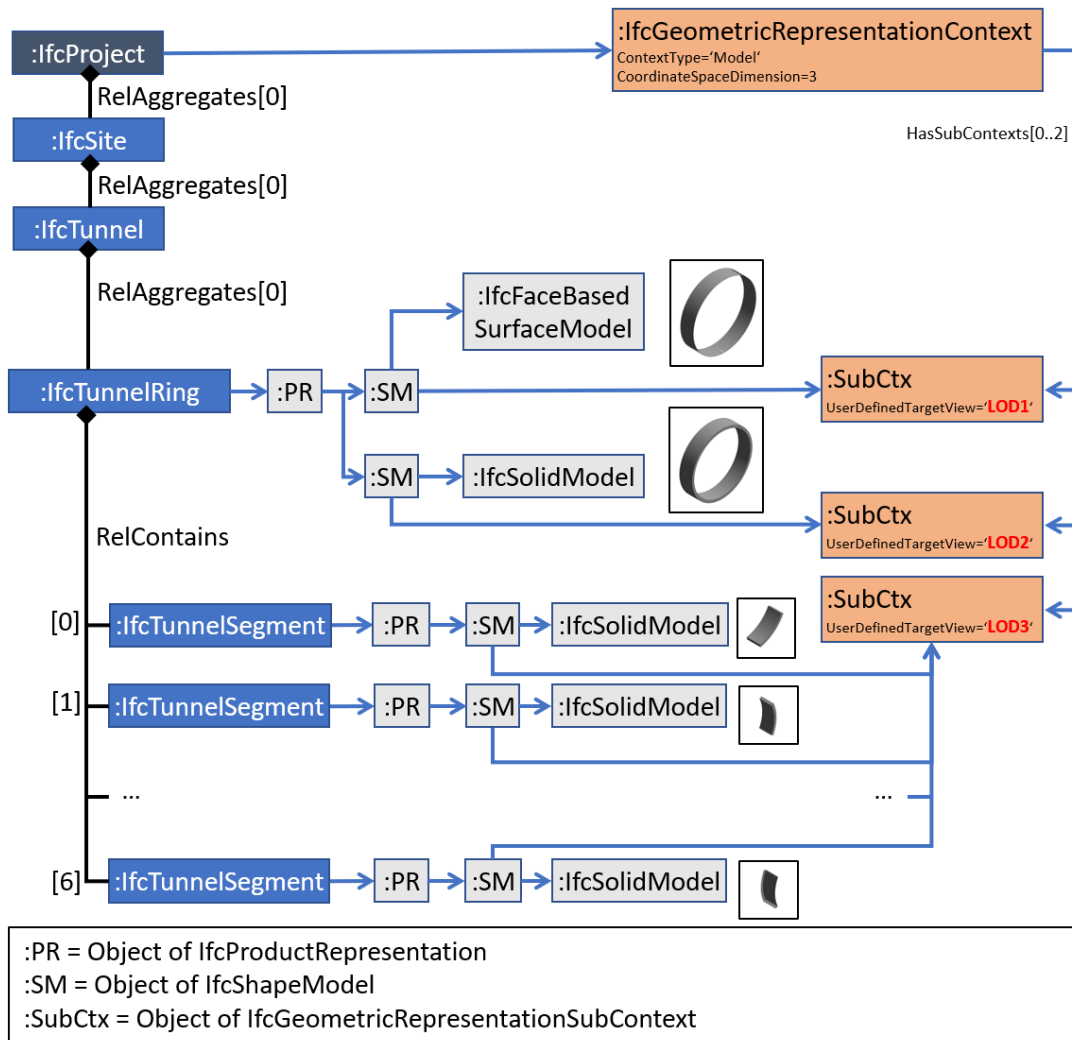
646 To exemplify the multi-level modelling approach, we present the object diagrams of one of the  
 647 building models and the tunnel lining model. Figure 21 outlines the object diagram for one of the  
 648 buildings. The spatial structure is restricted to the level of *IfcBuilding*. Here, the product  
 649 representation includes three different representations of subtype *IfcShapeModel*. The first,  
 650 representing geometry for LoD 1, just includes the footprint geometry of the building. The second,  
 651 representing geometry for LoD 2, includes an extrusion geometry. The last, representing the  
 652 geometry of LoD 3, includes a multitude of solid geometry elements to constitute the structural  
 653 model. To link properties to a specific LoD, these representations are assigned to instances of  
 654 *IfcGeometricRepresentationSubcontext*, whose value of the attribute *UserDefinedTargetView*  
 655 identifies the LoD, namely either "LOD1", "LOD2" or "LOD3".



656

657 Figure 21: Object diagram demonstrating IFC multi-level modelling of the tunnel lining

658 While the instantiation of one of the buildings models seems straightforward, the IFC  
 659 representation of the tunnel lining is more sophisticated. First of all, because the IFC domain  
 660 actually does not contain any specific classes within the domain of mechanized tunnelling, we  
 661 utilize an extension previously published in [1], containing the classes *IfcTunnel* and  
 662 *IfcTunnelRing*, inherited from *IfcSpatialStructureElement* as well as the class *IfcTunnelSegment*,  
 663 inherited from *IfcElement*. *IfcTunnel* represents the most upper spatial definition of the tunnel  
 664 lining, similar to the *IfcBuilding* class. It further decomposes into spatial structures for the tunnel  
 665 rings (*IfcTunnelRing*). The actual physical tunnel segments are finally represented by means of  
 666 *IfcTunnelSegment*. Figure 22 outlines the object diagram of the tunnel lining.

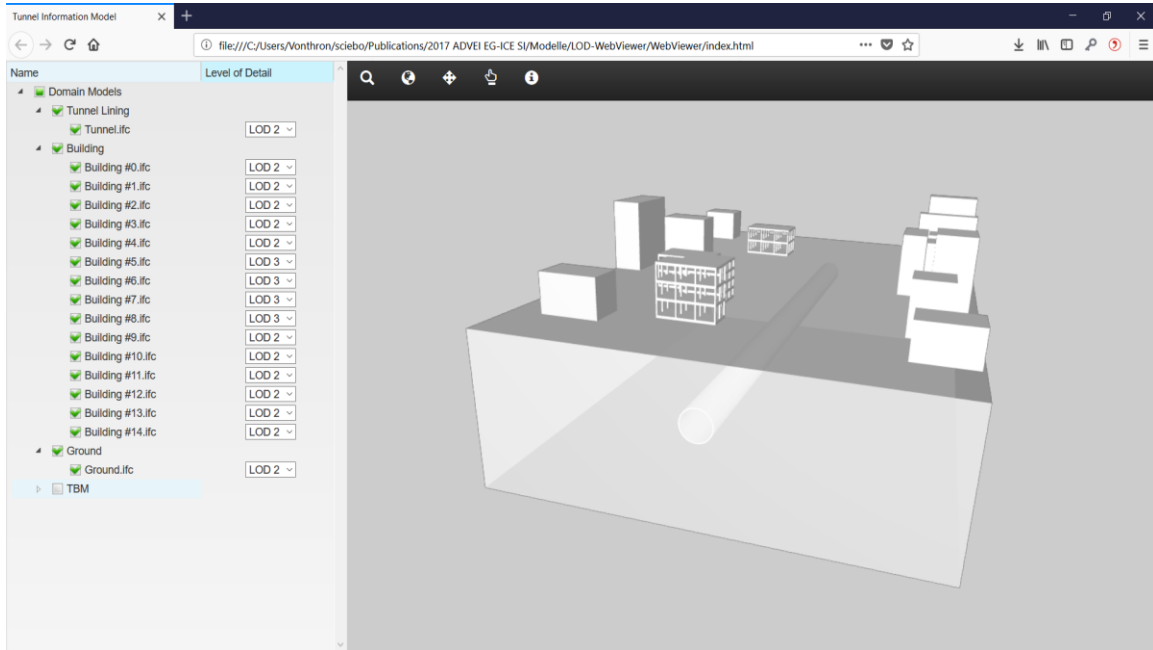


667

668 Figure 22: Object diagram demonstrating IFC multi-level modelling of the tunnel lining

669 When modelling the buildings, the geometries have been assigned to multiple representations  
 670 within the product representations of exactly one spatial structure instance (*IfcBuilding*). The  
 671 assignment within the tunnel lining model, however, further applies to multiple levels of spatial  
 672 structure. For the geometries of the lower levels, LoD 1 and LoD 2, a face model for the ring shell  
 673 and a solid model for the solid body of a tunnel ring have been both assigned as separate  
 674 representations to the spatial structure *IfcTunnelRing*. The corresponding contexts have been  
 675 linked, accordingly. In contrast, the geometries for representing segment geometry have been  
 676 assigned to separate physical elements of type *IfcTunnelSegment*, but all have been linked to the  
 677 same context object, which identifies LoD 3.

678 Since common IFC viewers do not yet distinguish multiple representation contexts, and thus would  
679 show all geometries at the same time, we extended the IFC Web-Viewer, which has been introduced  
680 in [1], to support such contexts. Figure 23 depicts the configuration of Model 2 (see Fig. 18 b,  
681 optimised LoD 2 and LoD 3), which in this case, has not been configured from scratch, but by  
682 selecting the proper representation context for each of the exported domain models, e.g. tunnel  
683 lining at LoD 2, and building #5 at LoD 3.



684

685 Figure 23: IFC Web-Viewer presenting model geometries from different LoD contexts

#### 686 4. CONCLUSIONS

687 Due to increasing urbanisation and mobility there is a need for the efficient and safe design and  
688 construction of mechanised tunnels using the latest computer-supported technologies, such as BIM  
689 and FE simulations. In this context, existing literature has shown the potential of multi-LoD  
690 information models and the need for advanced numerical simulation models. What was missing is  
691 the multi-LoD integration of the information and the numerical model.

692 This paper proposes a novel concept of parametric information modelling for multi-level decision  
693 support for mechanised tunnelling projects: SATBIM is an integrated, open-source platform for  
694 information modelling, structural analysis and visualisation. Within this platform, industry-  
695 standard tools (Autodesk Revit and Dynamo) are employed for the design of the tunnel structure

696 and the surrounding infrastructure with consideration of LoDs for all system components. Based  
697 on the multi-level parametric BIM, multi-level numerical models are developed for each  
698 component, considering proper geometric as well as material representation, interfaces and the  
699 representation of the construction process. The numerical models are then, fully automatically,  
700 instantiated and executed based on the BIM. Finally, the simulation outputs are read back and  
701 visualised within Revit.

702 SATBIM enables efficient design and assessment of design alternatives reducing the modelling  
703 efforts and computation time by: (i) minimisation of the efforts needed for model generation; (ii)  
704 representation at different LoDs leading to computationally efficient simulations; and (iii) effective  
705 visualisation of the simulation results. This modelling and computational efficiency is  
706 demonstrated in the numerical example presented in this paper. Applying the optimal LoDs of the  
707 components in the information models and automatically generating corresponding numerical  
708 simulations, have significantly reduced the computational efforts without affecting the accuracy of  
709 the assessment. Further improvement of the computational efficiency can be achieved by using  
710 parallelisation strategies or simulation-based meta models [54]. Moreover, the extension for  
711 representation of multiple LoD configurations of the TIM components into a single IFC file allows  
712 for interoperability of the proposed platform with other BIM tools in a structured and efficient way.

713 The list below summarises the major contribution of the work presented in this article:

- 714 • Concept and implementation of an integrated parametric multi-LoD information and numerical  
715 model for mechanised tunnelling that consistently links the corresponding LoD descriptions in  
716 both the information and the numerical worlds.
- 717 • Software framework that assists the:
  - 718 ○ semi-automated parametric generation of multi-LoD information models
  - 719 ○ automated generation and analysis of a specific-LoD numerical model
- 720 • Concept and implementation of a multi-LoD tunnel information model using the Industry  
721 Foundation Classes and their functionalities for relations modelling (LoD for the semantics of  
722 physical building elements) and for geometric representation contexts (LoD for the geometry of  
723 those elements)

724 The current framework employs FE analysis for the design assessment, and it is well-known that  
725 for high accuracy of the numerical solution, a fine discretisation of the FE mesh is required.  
726 Therefore, in order to achieve high accuracy of the solution at low computational costs, we aim to  
727 integrate Iso-Geometric Analysis (IGA) and make a direct use of the B-rep geometries generated  
728 in the BIM for the definition of numerical models. This concept has been proven as successful for

729 the tunnel lining component [56], and in the future development of our framework, we will work  
730 toward integration of design and IGA for the other tunnel components addressed in this study.  
731 Another limitation of the current state of development of the framework is the numerical  
732 representation of structures at the highest LoD, which at the moment is restricted to geometrical  
733 models of the structural frame using linear elastic material models. For more realistic representation  
734 of structures and the structural damage induced by tunnelling, our future work will involve  
735 development and implementation of damage models, as well as improvements in modelling of  
736 details such as connections between the structural elements. The SATBIM toolkit is made available  
737 as open source software together with technical report, and benchmark examples deposited in the  
738 Github repository: <https://github.com/satbim>.

739

740 **ACKNOWLEDGEMENTS**

741 The authors gratefully acknowledge the financial support by the European Union’s Horizon 2020  
742 research and innovation programme under the Marie Skłodowska-Curie grant agreement No  
743 702874 and the German Research Foundation (DFG) within the subproject D1 of the Collaborative  
744 Research Center SFB 837 “Interaction Modeling in Mechanised Tunnelling”.

- [1] C. Koch, A. Vonthron and M. König, “A tunnel information modelling framework to support management, simulations and visualisations in mechanised tunnelling projects,” *Automation in Construction*, vol. 83, pp. 78-90, 2017.
- [2] A. Borrmann, M. Flurl, J. Jubierre, R.-P. Mundani and E. Rank, “Synchronous collaborative tunnel design based on consistency preserving multi-scale models,” *Advanced Engineering Informatics*, vol. 28, no. 4, pp. 499-517, 2014.
- [3] H. Lai and X. Deng, “Interoperability analysis of IFC-based data exchange between heterogeneous BIM software,” *Journal of Civil Engineering and Management*, vol. 24, no. 7, pp. 537-555, 2018.
- [4] S. Lee and B. Kim, “IFC Extension for Road Structures and Digital Modeling,” *Procedia Engineering*, vol. 14, p. 1037–1042, 2011.
- [5] Y. Ji, A. Borrmann, J. Beetz and M. Obergruesser, “Exchange of Parametric Bridge Models Using a Neutral Data Format,” *Journal of Computing in Civil Engineering*, vol. 27, no. 6, pp. 593-606, 2013.
- [6] D. Rebolj, A. Tibaut, N. Cus-Babic, A. Magdic and P. Podbrenznik, “Development and application of a road product model,” *Automation in Construction*, vol. 17, no. 6, p. 719–728, 2008.
- [7] N. Yabuki, T. Aruga and H. Furuya, “Development and application of a product model for shield tunnels,” in *Proc. of the 30th Intl. Symposium on Automation and Robotics in Construction*, Montreal, 2013.
- [8] A. Borrmann, T. Kolbe, A. Donaubaue, H. Steuer, J. Jubierre and M. Flurl, “Multi-scale geometric-semantic modeling of shield tunnels for GIS and BIM applications,” *Computer-Aided Civil and Infrastructure Engineering*, vol. 30, no. 4, p. 263–281, 2015.
- [9] J. Abualdenien and A. Borrmann, “A meta-model approach for formal specification and consistent management of multi-LOD building models,” *Advanced Engineering Informatics*, vol. 40, pp. 135 -153, 2019.
- [10] A. (. I. o. Architects), “AIA contract document G202–2013, building information modeling protocol form,” AIA, Washington DC, 2013.
- [11] BIMForum, “Level of development specification guide,” 2013.
- [12] G. Meschke, J. Ninic, J. Stascheit and A. Alsahly, “Parallelized computational modeling of pile-soil interactions in mechanized tunneling,” *Engineering Structures*, vol. 47, pp. 35-44, 2013.
- [13] N. Do, D. Dias, P. Oreste and D.-M. I., “Three-dimensional numerical simulation for mechanized tunnelling in soft ground: the influence of the joint pattern,” *Acta Geotechnica*, vol. 9, no. 4, pp. 673-694, 2014.
- [14] J. Ninic and G. Meschke, “Model update and real-time steering of tunnel boring machines using simulation-based meta models,” *Tunnelling and Underground Space Technology*, vol. 45, pp. 138-152, 2015.
- [15] N. Nawari and M. Kuenstle, *Building Information Modeling: Framework for Structural Design*, CRC Press, 2015.
- [16] L. Svoboda, J. Novak, L. Kurilla and J. Zeman, “A framework for integrated design of algorithmic architectural forms,” *Advances in Engineering Software*, vol. 72, pp. 109 - 118, 2014.

- [17] M. Breitenberger, A. Apostolatos, B. Philipp, R. Wuechner and K. Bletzinger, "Analysis in computer aided design: Nonlinear isogeometric B-Rep analysis of shell structures," *Computer Methods in Applied Mechanics and Engineering*, vol. 284, pp. 401-457, 2015.
- [18] M. Rafiq and I. MacLeod, "Automatic structural component definition from a spatial geometry model," *Engineering Structures*, vol. 10, no. 1, pp. 37-40, 1988.
- [19] S. Boonstra, K. van der Blom, H. Hofmeyer, M. T. Emmerich, J. van Schijndel and P. de Wilde, "Toolbox for super-structured and super-structure free multi-disciplinary building spatial design optimisation," *Advanced Engineering Informatics*, vol. 36, pp. 86-100, 2018.
- [20] G. Meschke, S. Freitag, A. Alsahly, J. Ninic, S. S. and C. Koch, "Numerical Simulation in Mechanized Tunneling in Urban Environments in the Framework of a Tunnel Information Model," *Bauingenieur*, vol. 89, no. 11, pp. 457-466, 2014.
- [21] J. Ninic, S. Freitag and G. Meschke, "A hybrid finite element and surrogate modelling approach for simulation and monitoring supported TBM steering," *Tunnelling and Underground Space Technology*, vol. 63, pp. 12-28, 2017.
- [22] A. Alsahly, V. Gall, A. Marwan, J. Ninic, G. Meschke, A. Vonthron and K. M., "From Building Information Modeling to Real time Simulation in Mechanized tunneling," in *Proceedings of the World Tunneling Congress 2016*, San Francisco, 2016.
- [23] J. Amann, A. Borrmann, F. Hegemann, J. Jubierre, M. Flurl, C. Koch and M. Koenig, "A refined product model for shield tunnels based on a generalized approach for alignment representation," in *Proc. of the 1st International Conference on Civil and Building Engineering Informatics*, 2013.
- [24] J. Ninić and C. Koch, "Parametric multi-level tunnel modelling for design support and numerical analysis," in *EURO:TUN 2017 - IV International Conference on Computational Methods in Tunneling and Subsurface Engineering*, Innsbruck, Austria, 2017.
- [25] AUTODESK, "Autodesk Revit," 2017. [Online]. Available: <http://www.autodesk.co.uk/products/revit-family/>.
- [26] D. Toll, H. Zhu, A. Osman, W. Coombs, X. Li and M. Rouainia, "Information Technology in Geo-Engineering," in *Proc. of the 2nd International Conference on Information Technology in Geo-Engineering*, 2014.
- [27] D. Aldiss, M. Blac, D. Entwisle, D. Page and R. Terrington, "Benefits of a 3D geological model for major tunnelling works: An example from Farringdon, east-central London, UK," *Quarterly Journal of Engineering Geology and Hydrogeology*, vol. 45, no. 4, pp. 405-414, 2012.
- [28] F. Zobl and R. Marschallinger, "Subsurface geo building information modelling GeOBIM," *Geoinformatics*, vol. 8, no. 11, pp. 40-43, 2008.
- [29] O. Arnau and C. Molins, "Three dimensional structural response of segmental tunnel linings," *Engineering Structures*, vol. 44, no. 0, pp. 210-221, 2012.
- [30] S. Teachavorasinskun and T. Chub-Uppakarn, "Influence of segmental joints on tunnel lining," *Tunnelling and Underground Space Technology*, vol. 25, no. 4, pp. 490-494, 2010.
- [31] J. Burland and C. Wroth, "Settlement of buildings and associated damage," in *Proc. of the Conference on Settlement of Structures*, 1975.
- [32] A. B. Vesic, "Beams on Elastic Subgrade and the Winkler's Hypothesis," in *Proceedings of 5th International Conference of Soil Mechanics*, 1963.
- [33] D. Kolymbas, *Geotechnik - Tunnelbau und Tunnelmechanik*, Springer, 1998.

- [34] F. Nagel and G. Meschke, "An elasto-plastic three phase model for partially saturated soil for the finite element simulation of compressed air support in tunnelling," *International Journal for Numerical and Analytical Methods in Geomechanics*, vol. 34, pp. 605-625, 2010.
- [35] A. Alsahly, J. Stascheit and G. Meschke, "Advanced finite element modeling of excavation and advancement processes in mechanized tunneling," *Advances in Engineering Software*, vol. 100, pp. 198-214, 2016.
- [36] H. Yu, "CASM: a unified state parameter model for clay and sand," *International Journal for Numerical and Analytical Methods in Geomechanics*, vol. 48, pp. 773-778, 1998.
- [37] B. Maidl, M. Herrenknecht, U. Maidl and G. Wehrmeyer, *Mechanised Shield Tunnelling*, Ernst und Sohn, 2012.
- [38] N.-A. Do, D. Dias, P. Oreste and I. Djeran-Maigre, "Three-dimensional numerical simulation for mechanized tunnelling in soft ground: the influence of the joint pattern," *Acta Geotechnica*, vol. 9, no. 4, pp. 673 - 694, 2014.
- [39] T. Kasper and G. Meschke, "A 3D finite element model for TBM tunneling in soft ground," *International Journal for Numerical and Analytical*, vol. 28, pp. 1441-1460, 2004.
- [40] F. Nagel, J. Stascheit and G. Meschke, "Numerical simulation of interactions between the shield supported tunnel construction process and the response of soft, water saturated soils," *International Journal of Geomechanics (ASCE)*, vol. 12, no. 6, pp. 689-696, 2011.
- [41] A. Lambreggi, L. Rodriguez and R. Castellanza, "Development and validation of a 3D numerical model for TBM-EPB mechanised excavations," *Computers and Geotechnics*, vol. 40, pp. 97-113, 2012.
- [42] N.-A. Do, D. Dias, P. Oreste and I. Djeran-Maigre, "2D tunnel numerical investigation: The influence of the simplified excavation method on," *Geotechnical and Geological Engineering*, vol. 32, no. 1, pp. 43-58, 2014.
- [43] G. Meschke, "Consideration of aging of shotcrete in the context of a 3D viscoplastic material model," *International Journal for Numerical*, vol. 39, pp. 3123-3143, 1996.
- [44] T. Kasper and G. Meschke, "On the influence of face pressure, grouting pressure and TBM design in soft ground tunnelling," *Tunnelling and Underground Space Technology*, vol. 21, no. 2, pp. 160-171, 2006.
- [45] V. Founta, J. Ninic, A. Whittle, G. Meschke and J. Stascheit, "Numerical simulation of ground movements due to EPB tunnelling in clay," in *Prof. of the 3rd International Conference on Computational Methods in Tunneling and Subsurface Engineering (EURO:TUN 2013)*, Bochum, 2013.
- [46] F. Nagel and G. Meschke, "Grout and bentonite flow around a TBM: Numerical simulations addressing its impact on surface settlements," *Tunnelling*, vol. 26, pp. 445-452, 2011.
- [47] T. Laursen, *Computational Contact and Impact Mechanics*, Berlin-Heidelberg: Springer, 2002.
- [48] J. Waeytens, B. Rosić, P.-E. Charbonnel, E. Merliot, D. Siegert, X. Chapeleau, R. Vidal, V. le Corvec and L.-M. Cottineau, "Model updating techniques for damage detection in concrete beam using optical fiber strain measurement device," *Engineering Structures*, vol. 129, pp. 2-10, 2016.
- [49] S. Schindler and P. Mark, "Evaluation of building stiffness in the risk-assessment of structures affected by settlements," in *Proceedings of Third International Conference on Computational Methods in Tunneling and Subsurface Engineering*, Bochum, 2013.
- [50] M. Venugopal, C. Eastman, R. Sacks and J. Teizer, "Semantics of model views for information exchanges using the industry foundation class schema," *Advanced Engineering Informatics*, vol. 26, no. 2, pp. 411-428, 2012.

- [51] A. Melendo, A. Coll, M. Pasenau, E. Escolano and A. Monros, “GiD: the personal pre- and postprocessor,” 2017. [Online]. Available: <http://www.gidhome.com/>. [Accessed Januar 2018].
- [52] P. Dadvand and R. Rossi, “Kratos Multi-physics,” International Center for Numerical Methods in Engineering (CIMNE), 2017. [Online]. Available: <http://www.cimne.com/kratos/>. [Accessed Januar 2018].
- [53] J. Ninic, C. Koch and J. Stascheit, “An integrated platform for design and numerical analysis of shield tunnelling processes on different levels of detail,” *Advances in Engineering Software*, vol. 112, pp. 165-179, 2017.
- [54] J. Ninic, H. Bui, C. Koch and G. Meschke, “Computationally Efficient Simulation in Urban Mechanized Tunneling Based on Multilevel BIM Models,” *Journal of Computing in Civil Engineering*, vol. 33, no. 3, p. 04019007, 2019.
- [55] RDF, “IFC Engine,” 2017. [Online]. Available: <http://www.ifcbrowser.com/>. [Accessed 15 November 2017].
- [56] J. Ninic, H. Bui and M. G., “Parametric Design and Isogeometric Analysis of Tunnel Linings within the Building Information Modelling Framework,” in *EG-ICE 2019 Workshop on Intelligent Computing in Engineering*, Leuven, Belgium, 2019.

747

748

749